

Sinuuous bar fingers of digitate shallow-water deltas: Insights into their formative processes and deposits from integrating morphological and sedimentological studies with mathematical modelling

ZHENHUA XU^{*†}, PIRET PLINK-BJÖRKLUND[‡], SHENGHE WU^{*†} , ZHAO LIU[§], WENJIE FENG[¶], KE ZHANG^{*†}, ZHENG YANG^{*†} and YACONG ZHONG^{**}

^{*}State Key Laboratory of Petroleum Resources and Prospecting, China University of Petroleum-Beijing, Beijing, 102249, China (E-mail: reser@cup.edu.cn)

[†]College of Geosciences, China University of Petroleum-Beijing, Changping, Beijing, 102249, China (E-mail: reser@cup.edu.cn)

[‡]Department of Geology and Geological Engineering, Colorado School of Mines, 80401, USA

[§]Sinopec Geophysical Research Institute, Nanjing, 211103, China

[¶]School of Geoscience, Yangtze University, Wuhan, 434100, China

^{**}Geophysical Exploration Research Institute of COSL, Tianjin, 300450, China

Associate Editor – Massimiliano Ghinassi

ABSTRACT

This paper helps to address the growing need to resolve the severe loss of deltaic lands by providing a new understanding for shallow-water digitate delta growth. The integration of satellite image analysis of modern deltas, field studies of the Ganjiang Delta in the Poyang Lake and ‘Delft3D’ simulations further results in improved facies models for shallow-water digitate deltas. These analyses show that shallow-water digitate delta bar fingers are sinuous in contrast to the straight deep-water digitate delta bar fingers. These differences are assigned to the effect of water depth on outflow hydraulics, where friction-dominated shallow-water delta effluents promote mouth bar deposition that then divert flow around the mouth bar, resulting in the formation of sinuous bar fingers. These effects are further strengthened by the meandering of the shallow-water jet that increases lateral sediment transport, and by the higher flow resistance and lower gradient of the shallow-water outflows. Our data and analyses further show differences in the morphology and deposits of the shallow-water sinuous bar fingers, where some bar fingers develop sinuous and others meandering (with point bars) distributary channels. Lateral channel migration and point bar formation (meandering) occur as a secondary process that does not change the shape or width of the bar fingers themselves, and is suggested to be a function of slight initial differences in channel sinuosity. These differences in distributary channel morphology have a strong effect on bar finger facies distribution. Sediment cohesion is another important control on bar finger bending processes, because high cohesion promotes formation of enclosed bays, where their bank strength exceeds the centrifugal force of water flow. Lower sediment cohesion results in sinuous bar fingers without formation of enclosed bays. This work provides insights into natural and artificial shallow-water digitate delta growth and provides new quantitative facies models for shallow-water digitate deltas.

Keywords Delft3D simulation, depositional processes, digitate shallow-water deltas, facies models, sinuous bar fingers, the Ganjiang Delta in Poyang Lake.

INTRODUCTION

River deltas rank among the most economically and ecologically valuable environments on Earth and are increasingly vulnerable to coastal hazards and sea-level rise. Deltas also host abundant hydrocarbon reserves. Consequently, delta morphology and evolution, as well as deltaic facies distribution are of high interest (e.g. Caldwell *et al.*, 2019; Willis & Sun, 2019; Edmonds *et al.*, 2020; Nienhuis *et al.*, 2020).

River-dominated deltas can be divided into lobate and digitate deltas based on their morphological characteristics (Bernard, 1965; Fisher *et al.*, 1969; Dumars, 2002; Olariu & Bhattacharya, 2006; Burpee *et al.*, 2015; Marfai *et al.*, 2016), attributed to differences in dominant grain size and the proportion of cohesive sediment (Edmonds & Slingerland, 2010; Caldwell & Edmonds, 2014). Lobate geometries are suggested to result from numerous distributary channels and mouth bars that develop sheet sands in coarse-grained, low-cohesive deltas (Fisk, 1955; Dumars, 2002; Olariu & Bhattacharya, 2006; Caldwell & Edmonds, 2014). In contrast, fine-grained deltas (Fig. 1) are suggested to develop digitate bar fingers (*sensu* Bates, 1953; Fisk, 1955; Donaldson, 1974; Galloway, 1975; Kim *et al.*, 2009a; Rowland *et al.*, 2010) that consist of distributary channels, mouth bars and levées, where the latter transition into marshes and bays (Fig. 2) (Fisk, 1954, 1955, 1961; Donaldson, 1974; Kulp *et al.*, 2005). Bar fingers are the only positive landforms in digitate deltas, and determine the distribution of land. Understanding the bar finger morphology and dimensions, their distribution and evolution is consequently essential for prediction of the growth of natural or artificial deltas, such as prediction of artificial delta growth in the shallow bays near Mississippi Delta to resolve the severe loss of deltaic lands (Day *et al.*, 2000, 2007; Syvitski & Saito, 2007; Kim *et al.*, 2009b; Falcini *et al.*, 2012; Nittrouer *et al.*, 2012). Bar fingers also determine the facies and grain-size distributions, and the architecture of the digitate deltas, significant for the prediction of hydrocarbon reserves, such as targeted in many large

petroliferous shallow-water basins (for example, Ordos Basin – Hu *et al.*, 2008; Bohai Bay Basin – Zhang *et al.*, 2017, Xu *et al.*, 2019).

Deltas are further shown to develop different characteristics as a function of basinal water depth and gradient. Shallow-water deltas form in just a few metres of water depth (Fig. 1), such that the distributary channels are commonly deeper than the water depth at the distributary mouth (Edmonds *et al.*, 2011; Wu *et al.*, 2019). Deep-water deltas (for example, the Mississippi Delta) form in tens to hundreds of metres water depth, and the distributary channels are always shallower than the basinal water depth outside the distributary mouth.

This paper compares the morphology of bar fingers in deep-water and shallow-water deltas, and shows that *bar fingers in shallow-water deltas (BSDs)* strongly trend to be sinuous, whereas the *bar fingers in deep-water deltas (BDDs)* strongly trend to be straight (Fig. 1) (see also Edmonds & Slingerland, 2010; Burpee *et al.*, 2015; Tejedor *et al.*, 2016; Xu *et al.*, 2019). This article further quantifies the morphology and deposits of the *BSDs* from satellite images of nine deltas (Fig. 1) and field data from the Ganjiang Delta (Fig. 3), and studies the evolution of *BSDs* by mathematical modelling (Delft3D). It is shown that *BSDs* develop different sinuosities and different sinuosity ratios with their distributary channels, and facies models are proposed for these different types of *BSDs*. Further, it is shown that *BSDs* create distinct land building patterns, and the following questions are addressed: (i) what are the bending mechanisms of the *BSDs*; (ii) what causes the differences in *BSD* sinuosity and *BSD* to distributary channel sinuosity ratio; (iii) what is the role of cohesion in *BSD* bending mechanisms; and (iv) what are the processes that promote straight *BDDs* and sinuous *BSDs*?

DATASET

This paper integrates satellite image analysis, sedimentological fieldwork, and Delft3D simulations to analyze the morphology, architecture

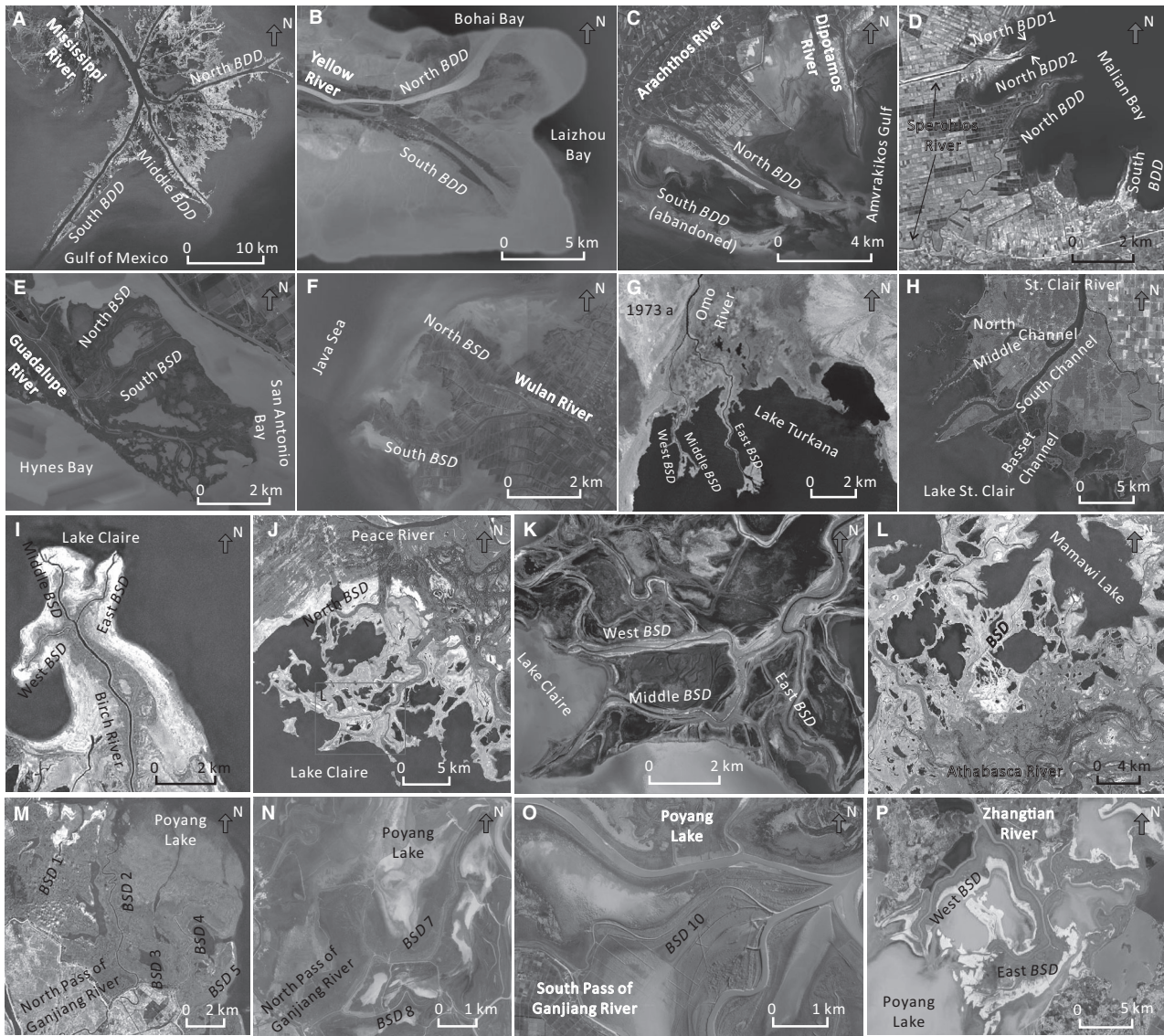


Fig. 1. Landsat images of some of the documented digitate deltas. Deep-water deltas: Mississippi Delta, Gulf of Mexico, USA (A); Yellow River Delta, Bohai Sea, China (B); Arachthos River Delta and Dipotamos River Delta, Amvrakikos Gulf, Greece (C); Sperchios River Delta, Malian Bay, Greece (D). Shallow-water deltas: Guadalupe Delta, San Antonio Bay, USA (E); Wulan Delta, Java Sea, Indonesia (F); Omo River Delta, Lake Turkana, Ethiopia (G); St Clair River Delta, Lake St Clair, USA and Canada (H); Birch River Delta, Lake Claire, Canada (I); Peace-Athabasca Delta, Lake Claire, Canada (J) to (L); Ganjiang Delta (M) to (O) and Zhangtianhe Delta (P), Poyang Lake, China.

and depositional process of the sinuous *BSDs*. Modern *BSDs* are globally widely distributed and were documented from readily available high-definition satellite images (Fig. 1). Data are used from nine shallow-water and nine deep-water deltas, from 31 *BSDs* and 24 *BDDs*, respectively (Fig. 1, Table 1). Sedimentary data was collected from 10 *BSDs* from the Ganjiang Delta in the Poyang Lake, Jiangxi Province, China (Fig. 3A).

The Ganjiang Delta is a typical shallow-water delta with the average ratio of the distributary channel depth to the water depth at distributary mouth of 1.3. The Poyang Lake, the largest freshwater lake in China, is located on the southern bank of the Yangtze River (Fig. 3A). The Poyang Lake formed approximately at 400 AD, and is 110 km long and 50 to 70 km wide (Xu *et al.*, 2001), covering an area of 4125 km² (Shankman *et al.*, 2006). The lake

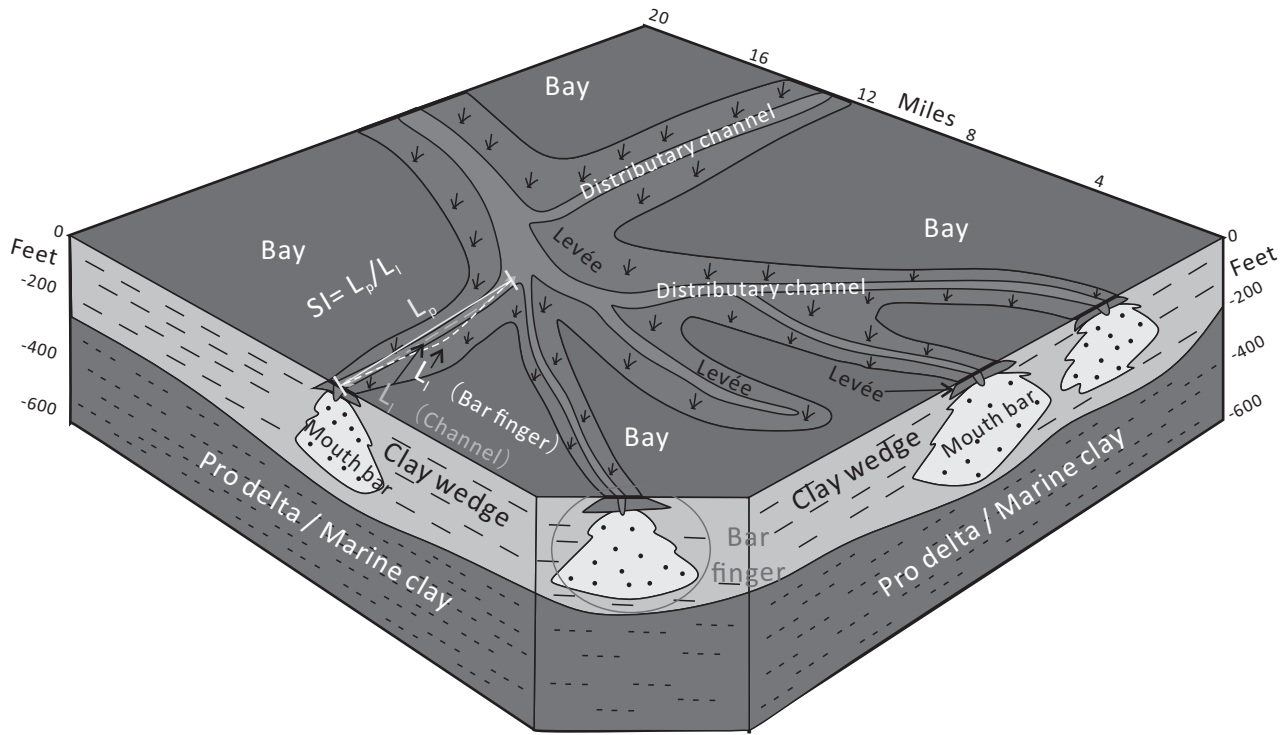


Fig. 2. Morphological and facies model of bar fingers in digitate deltas, based on the Mississippi Delta (modified from Fisk, 1954).

bottom has a gentle gradient of $<0.1^\circ$, average water depth of 8.4 m, and the wave and tide processes are weak (Yin & Zhang, 1987). The Ganjiang, Fuhe, Raohe, Xinjiang and Xiushui rivers (Fig. 3A) flow into the Poyang Lake and then out into the Yangtze River during wet seasons (Tan, 1982). The Yangtze River flows into the Poyang Lake during dry seasons (Hu, 1999). The Ganjiang River is the largest river in the Jiangxi Province, and flows into the western side of the lake where it forms the Ganjiang Delta (Fig. 3), which is the largest delta in the Poyang Lake. The Ganjiang River bifurcates at Nanchang into four distributary channels (Fig. 3). Sedimentary environments in the Ganjiang Delta can be divided into upper and lower delta plain, delta front and prodelta (Fig. 4) (Jin *et al.*, 2011). The upper delta plain is subaerial even during flood season and bounded downstream by artificial levées (pink dashed lines in Fig. 4). The boundary between the lower delta plain and delta front, and prodelta is defined by the basinward termination of subaerial bars during dry season (yellow dashed line in Fig. 4). The Ganjiang Delta contains a lobate delta, as well as *BSDs* (Fig. 4). Numerous previous

studies have focused on the lobate part of the Ganjiang Delta (e.g. Huang *et al.*, 2013; Jin *et al.*, 2011, 2017; Duan *et al.*, 2014; Gao *et al.*, 2016; Li *et al.*, 2016; Feng *et al.*, 2017; Zhang *et al.*, 2020), but the *BSDs* are unexplored.

Artificial levées, built in the 1960s, leaves *BSDs* on the lower delta plain and delta front essentially abandoned. The sediments of the Ganjiang River are mostly blocked by the artificial levées, and only some fine-grained suspended sediments flow over the levée during the flood season and are deposited at the top of the artificial levées. The artificial levées also increase the water level of Poyang Lake during the flood season, which promotes levée aggradation.

METHODS

Satellite image analysis

This study uses satellite images to quantify the sinuosity of bar fingers and distributary channels, using the *sinuosity index* (SI) of Rust (1978) originally defined for rivers:

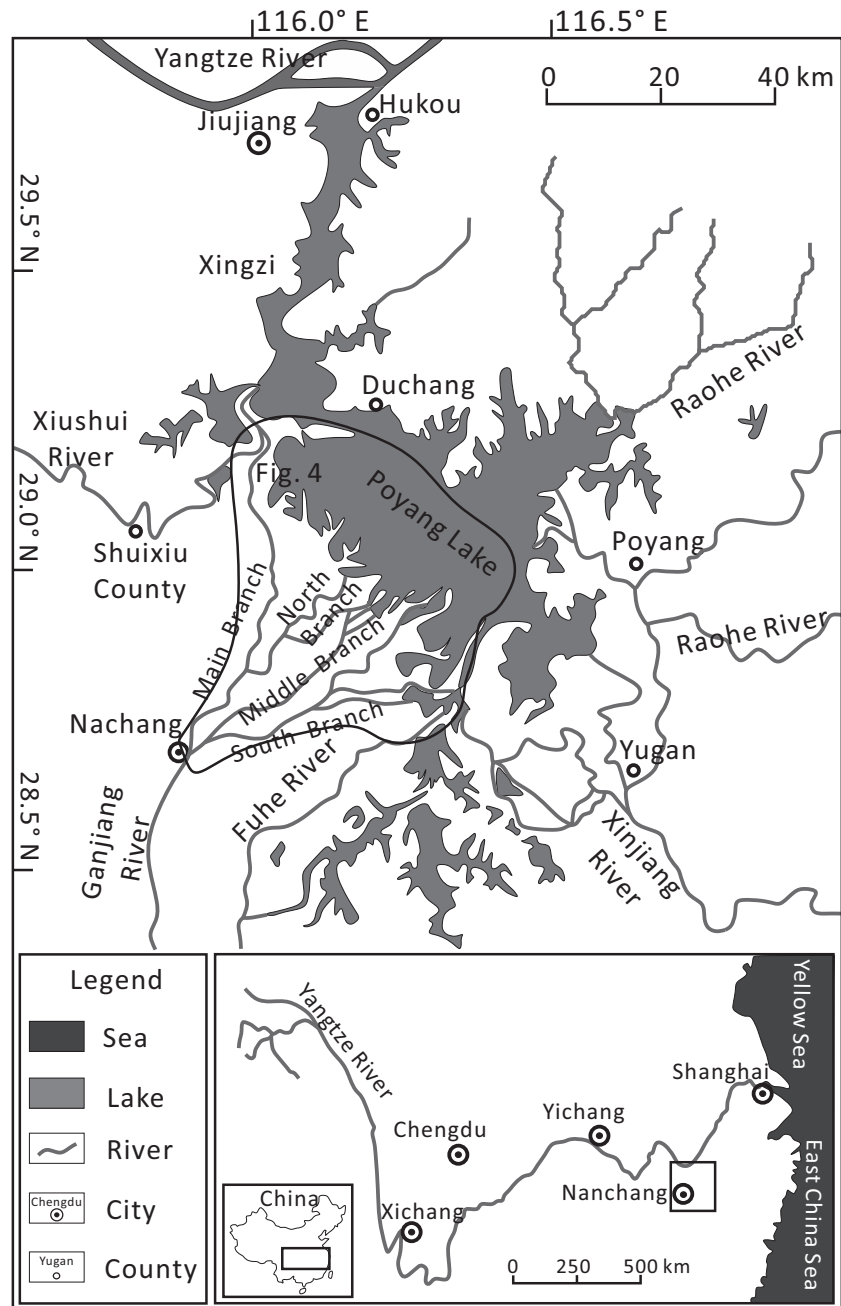


Fig. 3. Map of the Poyang Lake with rivers and distributaries (modified from Shankman *et al.*, 2006).

$$SI = \frac{L_p}{L_l} \quad (1)$$

where L_p is the physical length down the axis of the central line and L_l is the Euclidean distance (straight distance) between the end points of the distributary channel or bar finger (Fig. 2). Bar fingers and distributary channels are considered straight when $SI < 1.1$, and sinuous when $SI \geq 1.1$ (Woodbridge, 2013). The authors consider the bar fingers and distributary channels

meandering when $SI > 1.25$ (Brice & Blodgett, 1978). This metric, rather than the 1.5 of Bridge (2003) is used because point bars occur in this dataset in channels with $SI \geq 1.2$, and their average SI is 1.37. The non-parametric Mann-Whitney and Kolmogorov-Smirnov tests are used to test the statistical difference between the groups of sinuosity data, by asymptotic significance values (Usman, 2016), where values of < 0.05 represent the significant difference between the groups.

Table 1. The *sinuosity index* (SI) values of bar fingers and distributary channels in studied digitate deltas. The following data are from: ¹Donaldson (1974); ²Timoney & Lee (2016); ³Thomas *et al.* (2006); ⁴Marfai *et al.* (2016); ⁵Fadlillah *et al.* (2019); ⁶Avery & Tebbs (2018); ⁷Fisk (1954, 1955); ⁸Li *et al.* (1998); ⁹Poulos *et al.* (1993); ¹⁰Drosou *et al.* (2015); ¹¹Rao *et al.* (1990); ¹²Kumari & Rao (2009); and ¹³Kostianoi & Kosarev (2005).

Modern deltas		SI of distributary channel			
		Upper delta plain	Lower delta plain to delta front	SI of bar finger	Water depth ratio
Ganjiang Delta (Poyang Lake)	<i>BSD1</i>	1.16	1.34	1.20	1.3
	<i>BSD2</i>	1.32	1.36	1.18	1.3
	<i>BSD3</i>	1.16	1.40	1.22	1.3
	<i>BSD4</i>	1.16	1.39	1.26	1.3
	<i>BSD5</i>	1.16	1.72	1.40	1.3
	<i>BSD6</i>	1.16	1.20	1.22	1.3
	<i>BSD7</i>	1.31	1.14	1.15	1.3
	<i>BSD8</i>	1.12	1.49	1.32	1.3
	<i>BSD9</i>	1.12	1.41	1.26	1.3
	<i>BSD10</i>	1.07	1.30	1.20	1.3
Zhangtianhe Delta (Poyang Lake)	West <i>BSD</i>	1.16	1.32	1.25	1.3
	East <i>BSD</i>	1.16	1.82	1.58	1.3
East Guadalupe Delta (San Antonio Bay)	North <i>BSD</i>	1.16	1.12	1.13	2.5 ^[1]
	South <i>BSD</i>	1.16	1.18	1.20	2.5 ^[1]
Birch River Delta (Lake Claire)	West <i>BSD</i>	1.07	1.27	1.30	1.5 ^[2]
	Middle <i>BSD</i>	1.07	1.15	1.18	1.5 ^[2]
	East <i>BSD</i>	1.07	1.12	1.14	1.5 ^[2]
Western Peace delta (Lake Claire)	North <i>BSD</i>	1.45	1.51	1.29	1.0 ^[2]
	West <i>BSD</i>	1.61	1.27	1.18	1.0 ^[2]
	Middle <i>BSD</i>	1.61	1.24	1.16	1.0 ^[2]
	East <i>BSD</i>	1.61	1.48	1.36	1.0 ^[2]
Athabasca Delta (Mamawi Lake)	<i>BSD</i>	1.74	1.22	1.08	1.0 ^[2]
St Clair River Delta (Lake St Clair)	North <i>BSD</i>	1.15	1.14	1.20	3.7 ^[3]
	Middle <i>BSD</i>	1.21	1.13	1.17	3.7 ^[3]
	South <i>BSD</i>	1.02	1.20	1.15	3.7 ^[3]
	Basset <i>BSD</i>	1.02	1.17	1.07	3.7 ^[3]
Wulan Delta (Java Sea)	North <i>BSD</i>	1.06	1.13	1.15	1.0 ^[4, 5]
	South <i>BSD</i>	1.06	1.16	1.14	1.0 ^[4, 5]
Omo River Delta (Lake Turkana)	West <i>BSD</i>	1.20	1.39	1.27	1.1 ^[6]
	Middle <i>BSD</i>	1.23	1.31	1.18	1.1 ^[6]
	East <i>BSD</i>	1.20	1.34	1.30	1.1 ^[6]
Mississippi Delta (Gulf of Mexico)	South <i>BDD</i>	1.40	1.02	1.02	0.2 ^[7]
	Middle <i>BDD</i>	1.40	1.02	1.04	0.2 ^[7]
	North <i>BDD</i>	1.40	1.04	1.04	0.2 ^[7]
Yellow River Delta (Laizhou Bay)	North <i>BDD</i>	1.19	1.07	1.07	0.3 ^[8]
	South <i>BDD</i>	1.19	1.02	1.02	0.3 ^[8]
Aksiou delta (Aegean Sea)	West <i>BDD</i>	1.06	1.05	1.04	0.3 ^[9]
	Middle <i>BDD</i>	1.06	1.01	1.01	0.3 ^[9]
	East <i>BDD</i>	1.06	1.09	1.06	0.3 ^[9]
Aliakmona Delta (Aegean Sea)	West <i>BDD1</i>	1.63	1.02	1.02	0.2 ^[9]
	West <i>BDD2</i>	1.63	1.06	1.04	0.2 ^[9]
	Middle <i>BDD</i>	1.17	1.03	1.04	0.2 ^[9]
	East <i>BDD</i>	1.17	1.01	1.01	0.2 ^[9]

Table 1. (continued)

Modern deltas		SI of distributary channel			
		Upper delta plain	Lower delta plain to delta front	SI of bar finger	Water depth ratio
Sperchios River Delta (Malian Bay)	North <i>BDD1</i>	-	1.08	1.08	0.1 ^[9]
	North <i>BDD2</i>	-	1.01	1.01	0.1 ^[9]
	Middle <i>BDD</i>	1.20	1.10	1.08	0.1 ^[9]
	South <i>BDD</i>	1.33	1.04	1.04	0.1 ^[9]
Arachthos River Delta (Amvrakikos Gulf)	North <i>BDD</i>	1.35	1.02	1.01	0.3 ^[9, 10]
	South <i>BDD</i>	1.35	1.00	1.00	0.3 ^[9, 10]
Dipotamos River Delta (Amvrakikos Gulf)	<i>BDD</i>	1.18	1.02	1.02	0.2 ^[9]
Krishna Delta (Bay of Bengal)	West <i>BDD</i>	1.17	1.03	1.03	0.3 ^[11,12]
	Middle <i>BDD</i>	1.17	1.05	1.05	0.3 ^[11,12]
	East <i>BDD</i>	1.17	1.09	1.09	0.3 ^[11,12]
Ural River Delta (Caspian Sea)	North <i>BDD</i>	1.11	1.00	1.00	0.5 ^[13]
	South <i>BDD</i>	1.11	1.09	1.06	0.5 ^[13]

Both distributary channels and their corresponding bar fingers are sinuous, and their sinuosities differ. The *sinuosity ratio* (R_{SI}) is proposed to characterize this difference, defined as:

$$R_{SI} = \frac{SI_d}{SI_b} \quad (2)$$

where SI_d is the SI of the distributary channel, and SI_b is the SI of the bar finger. SI_d was measured both on lower-delta plain, and upper-delta plain and delta front (Table 1).

Field work

A field study in the Ganjiang Delta documents sedimentary facies, architecture and surficial morphology of the distributary channels, levées, point bars, mouth bars and inter-distributary bays of *BSDs*. Ganjiang Delta sand distribution was mapped from the delta plain to the delta front based on stratigraphic columns, and combined with a base map generated from modern and historical satellite images (Fig. 4). Stratigraphic columns were measured at a centimetre scale, using shallow core (Fig. 5A) drilled by a portable vibrating drilling machine (Fig. 5B) and exploratory pits (Fig. 5C). Further, multiple cross-sections were generated, and the dimensions of distributary channel, mouth bar, levée and point bar deposits in *BSD5* and *BSD6* (Fig. 4) were quantified. The widths of mouth bar and bar finger are all bottom width, and distributary channel width is bankfull width.

Production dates on buried trash (primarily food packaging bags) were used to estimate approximate age of deposition. These dates were then used to estimate approximate deposition rates in some levées where the buried trash occurs at multiple stratigraphic intervals.

Delft3D simulations

The *BSDs* were simulated with Delft3D (Version 4.01.01), software effective for simulation of delta depositional processes (Edmonds & Slingerland, 2010; Geleynse *et al.*, 2011; Caldwell & Edmonds, 2014; Burpee *et al.*, 2015). Delft3D is a numerical fluid-flow and sediment-transport model (Lesser *et al.*, 2004; Marciano *et al.*, 2005), which solves the depth-averaged, non-linear, shallow-water equations, sediment transport equations, and momentum and mass conservation equations (Burpee *et al.*, 2015). Flow is computed by solving the depth-integrated, Reynolds-averaged Navier-Stokes equations (Caldwell & Edmonds, 2014), which neglect the influences of evaporation, precipitation, Coriolis force, wind and waves (Lesser *et al.*, 2004; Dissanayake *et al.*, 2009).

In the Delft3D model, fine sediments (diameter $<64 \mu\text{m}$) are considered as cohesive sediments transported in suspension, whereas coarse sediments (diameter $>64 \mu\text{m}$) are considered as non-cohesive sediments transported as suspended or bedload. Cohesive sediments are essential for the formation of bar fingers (Edmonds & Slingerland, 2010). Formulation

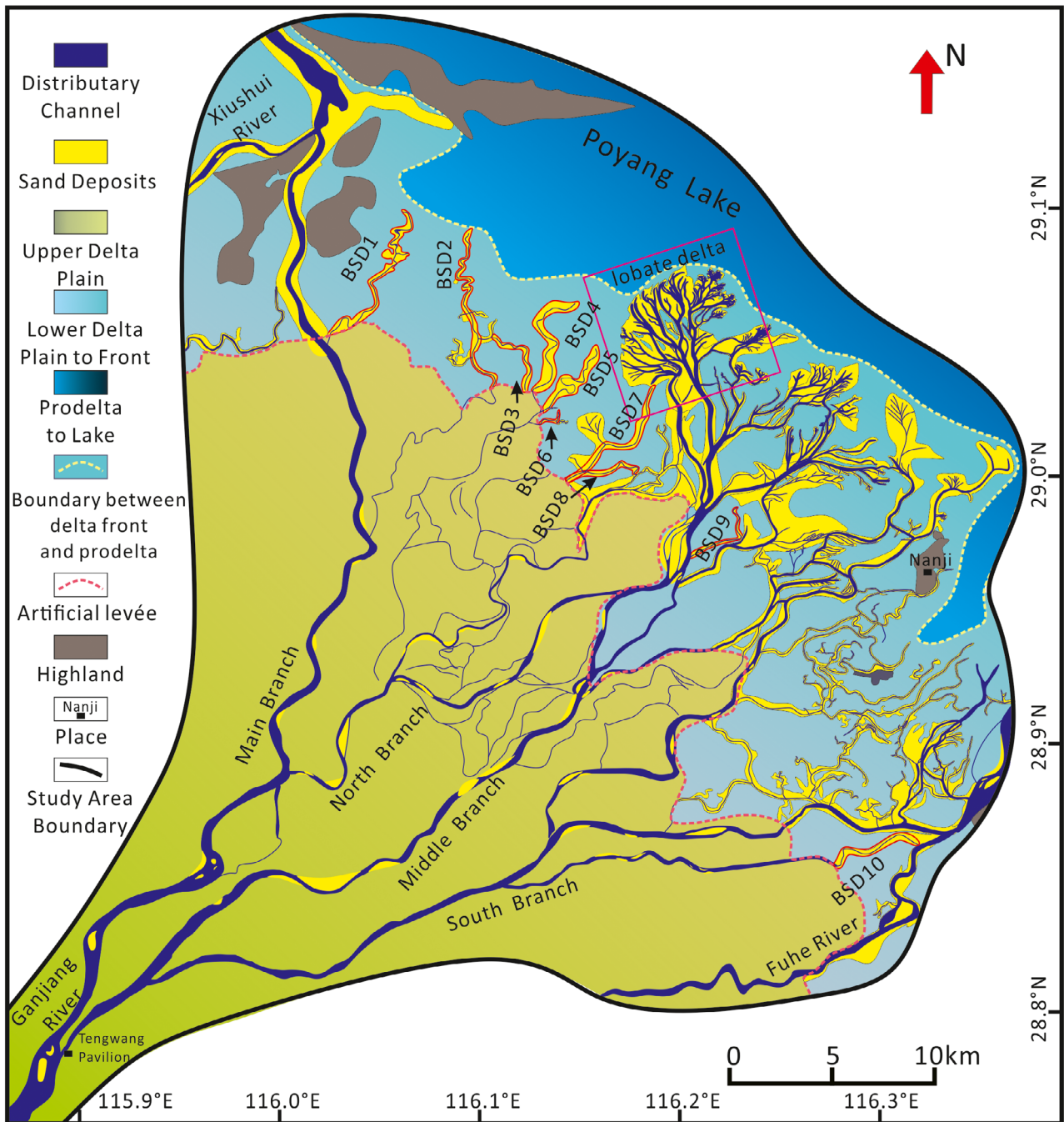


Fig. 4. Map of the shallow-water Ganjiang Delta, including sand distribution in bar fingers. Ten bar fingers (BSDs) and a lobate delta lobe are labelled and marked with red lines. Location of the Ganjiang Delta is shown in Fig. 3.

from van Rijn (1993) is adopted to calculate sediment transport mode as suspended or bedload. Direction of bedload transport affects the progradation, bifurcation or avulsion of distributary channels and bars, and is determined by local flow conditions as a function of bed-slope effects (Bagnold, 1966; Ikeda, 1982), predicted

by the determination of van Rijn (1993) and slope parameterization of Ikeda (1982) (see Baar *et al.*, 2019). The transverse bed slope parameter determines the amount of sediment transported sideways in channels, and may affect channel depth and bar dimensions (Van der Wegen & Roelvink, 2012; Schuurman *et al.*, 2013; Baar *et*



Fig. 5. An example of a core column (A) obtained by shallow drilling equipment (B) and an exploratory pit (C) from the Ganjiang Delta.

al., 2019). Transverse slope parameterizations 1.5 to 100 were tested and the default value 1.5 was chosen because the parameterization values had little effect on sinuosity and on other geomorphic parameters, including channel overdeepening.

Linking field observations with Delft3D simulations

Field observations and modelling were linked by using the satellite and the Ganjiang Delta data for simulation parametrization. The simulation area is 7500×5625 m with 25×25 m grid cells (Fig. 6), with initial basal bed slope of 3.75×10^{-4} . The initial river, 250 m long, 500 m wide and 2.5 m deep, is in the centre of the land area (Fig. 6). The Ganjiang River water discharge of $1200 \text{ m}^3 \text{ s}^{-1}$ and sediment concentration of 0.1 kg m^{-3} were used (Feng *et al.*, 2017), and kept steady, and the shallow-water basin had no waves or tides. Based on the Ganjiang Delta sediment samples, a mixture of six grain size classes with grain diameters of 300, 150, 80, 32, 13 and $7.5 \mu\text{m}$, in proportions of 3%, 3%, 4%, 30%, 30% and 30%, respectively, were used (Fig. 7). As high sediment cohesion, and thus high critical shear stress for the erosion of the cohesive sediment $[\tau_{ce}(c)]$, is important for the formation of BSDs (Edmonds & Slingerland, 2010), and the $\tau_{ce}(c)$ values from the Ganjiang Delta are

unknown, a range of $\tau_{ce}(c)$ values of 0.25, 1, 2 and 3.25 N m^{-2} were used in four simulations (S1 to S4). Discharge and water level variations, such as during floods, were not considered and this may reduce the frequency of avulsions (Wang *et al.*, 2020), whereas some BSDs in the Ganjiang Delta have avulsed a few times.

All simulations ran for 400 simulated hours with a time step of 0.2 min. The morphological scale factor 175 was used to allow an increased rate of morphological changes (Burpee *et al.*, 2015). Assuming that rivers experience bankfull (i.e. geomorphically effective) conditions 10 days per year (Caldwell & Edmonds, 2014), the simulation represents a period of 292 years (calculated from $400 \text{ h}/24 \text{ h per day} \times 175/10 \text{ days per year}$).

BAR FINGERS AND DISTRIBUTARY CHANNELS IN SHALLOW-WATER DELTAS: SINUOSITY

Distributary channel sinuosity on the upper delta plain is similar in shallow-water and deep-water deltas, with the average SI a little higher (1.22 versus 1.25) in deep-water deltas (Fig. 8). On lower delta plain and delta front, distributary channel sinuosity is considerably higher in shallow-water deltas with SI values >1.10 , and an average SI value of 1.30, as compared to $\text{SI} \leq 1.10$, and an average of 1.04 in deep-water deltas. Bar

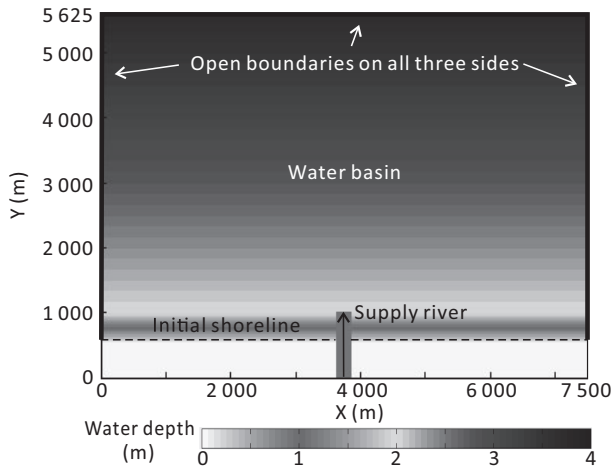


Fig. 6. Map view of the Delft3D model setup. Grid cells are 25×25 m. Black arrow indicates the flow direction of the river. Heavy solid lines are open boundaries.

finger sinuosity has also higher SI values in shallow-water deltas, with >1.07 , and an average of 1.22, as compared to $SI < 1.09$ and an average of 1.04 in deep-water deltas (Fig. 8). The non-parametric Mann–Whitney and Kolmogorov–Smirnov test results in the asymptotic significance values of <0.05 , and indicates that on lower delta plain and delta front the SI populations of bar fingers and distributary channels in shallow-water and deep-water deltas statistically differ.

There is a positive correlation between the SI of distributary channels (SI_d) and the SI of their bar fingers (SI_b) (Fig. 9). R_{SI} is defined as the ratio between SI_d and SI_b (SI_d/SI_b) to distinguish two types of linear positive relationships (Fig. 9); the high- R_{SI} ($R_{SI} > 1$) and low- R_{SI} ($R_{SI} \leq 1$) *BSDs*. The correlation coefficient is 0.88 for high- R_{SI} and 0.91 for low- R_{SI} *BSDs* (Fig. 9). High- R_{SI} *BSDs* are more common in the studied modern deltas than low- R_{SI} *BSDs*, where the high- R_{SI} ranges 1.02 to 1.23 and low- R_{SI} 0.95 to 0.99. The high- R_{SI} *BSDs* have higher-sinuosity distributary channels with SI_d values of ≥ 1.2 (with one exception) and average SI_d values of 1.37. The low- R_{SI} *BSDs* have lower-sinuosity distributary channels with SI_d values of 1.1 to 1.2 (with two exceptions) and average SI_d values of 1.16 (Fig. 9). Distributary channels are sinuous in low- R_{SI} *BSDs* and mostly meandering within high- R_{SI} *BSDs*. In the Ganjiang Delta, *BSD6* and *BSD7* have low- R_{SI} , and *BSD1–BSD5*, *BSD8–BSD10* have high- R_{SI} .

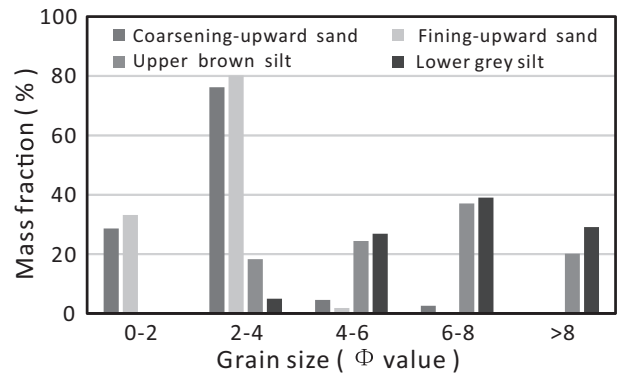


Fig. 7. Grain-size distribution of the four types of sandy/silty deposits of bar fingers (*BSDs*) from the Ganjiang Delta.

BAR FINGERS IN SHALLOW-WATER DELTAS: SEDIMENTOLOGY

Typical low- R_{SI} (*BSD6*) and high- R_{SI} *BSDs* (*BSD4*, *BSD5* and *BSD10*) were studied in detail to characterize their facies and architecture. *BSDs* are 10 km long but only 100 to 400 m wide and 0.3 to 2.0 m thick, and consist of fine-grained and medium-grained sand and mud (Fig. 10). Distributary channel deposits consist of medium sand overlain with silty sand and dark mud with plant fragments (Fig. 10; Table 2). The crescent-shaped point bars display accretion sets at the inner bank, and consist of scour-based upward fining brown or grey medium to fine sand with trough and wedge-shaped cross-strata. The flat-based and convex-up mouth bars consist of grey upward-coarsening grey fine to medium sand with tabular cross-strata and planar laminations. Levées at channel banks are affected by both river and lake flooding, and consist of upward fining brown rooted alternating silty sands and muds. The low parts of the terrain, the inter-distributary bays contain dark muds with plant fragments.

BAR FINGERS IN SHALLOW-WATER DELTAS: DEPOSITIONAL ARCHITECTURE AND MORPHOLOGY

BSD6 and *BSD5* were studied in detail to quantify depositional architecture and morphology of low- R_{SI} and high- R_{SI} *BSDs* (Figs 11 and 12). The low- R_{SI} (*BSD6*) and high- R_{SI} (*BSD5*) *BSDs* are similar in that they both consist of distributary channel, mouth bar and levée deposits. The difference is that *BSD5* also contains point bar

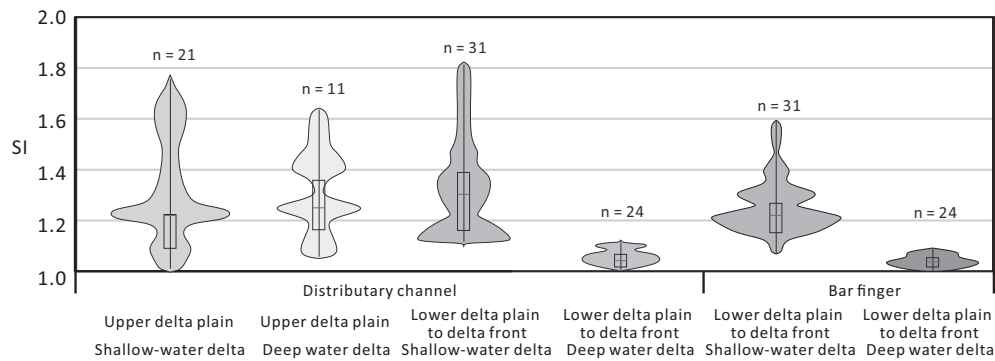


Fig. 8. The violin plots of the *sinuosity index* (SI) of distributary channels and bar fingers of digitate deep- and shallow-water deltas. On upper delta plain deep- and shallow-water deltas have similar sinuosity. On lower delta plain and delta front, shallow-water deltas have higher sinuosity distributary channels and bar fingers.

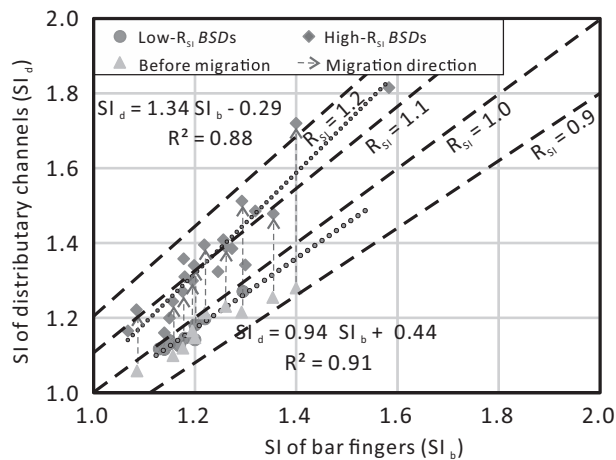


Fig. 9. Relationship between the *sinuosity index* (SI) of bar fingers (*BSDs*) and distributary channels. The ratio between SI of *BSDs* and distributary channels (R_{SI}) divides the bar fingers into high- R_{SI} ($R_{SI} > 1$) and low- R_{SI} ($R_{SI} \leq 1$) types. Triangles indicate the reconstructed sinuosity ratios of the high- R_{SI} distributary channels before they became meandering and formed point bars (see text for details).

deposits. The flat-based and convex-up mouth bars, up to 0.5 to 1.0 m thick and 200 to 300 m wide form the dominant sandy facies, and characteristically thin laterally (Figs 11 and 12). Where distributary channels, up to 0.3 to 2.5 m deep and 10 to 30 m wide, incise the mouth bars, the mouth bars become wing-shaped. The levée deposits, up to 0.4 to 1.5 m thick and 200 to 300 m wide, occur at distributary banks and also overlay the mouth bar deposits (Figs 11 and 12). The levées are thinner (<0.2 m in *BSD6* and <1.2 m in *BSD5*) where the mouth bars are

thickest (0.3 to 1.0 m), and also thin towards the margins of the *BSDs*, away from the channels. Mouth bar and levée width and thickness, and distributary channel incision depths decrease downstream (Figs 11 and 12). Mouth bars decrease from 300 to 10 m wide and from 1.0 to 0.3 m thick in *BSD5*, and from 200 to 50 m wide and from 0.5 to 0.1 m thick in *BSD6*. Levées decrease from 300 to 10 m wide and from 1.5 to 0 m thick in *BSD5*, and from 200 to 50 m wide and from 0.4 to 0 m thick in *BSD6*. Distributary channel incision depths decrease from 2.5 to 0.3 m in *BSD5* and from 1.0 to 0.2 m in *BSD6*. Decreasing *Cyperaceae* heights (from 0.8 to 0.2 m in *BSD5* and from 0.5 to 0.05 m in *BSD6*) indicate that the elevation of banks also decreases downstream by more than 0.5 m (Figs 13 and 14). The sinuosity of *BSDs* also decreases downstream, from SI 3.92 to 1.14 (Fig. 12). At the termination the *BSDs*, the distributary channels incise more at the centre of the mouth bars and the silty levée deposits pinch out (Figs 11 and 12).

The following sections below describe the differences in sinuosity, presence of point bars, incision depth of distributary channels, and levée thickness of low- R_{SI} (*BSD6*) and high- R_{SI} (*BSD5*) *BSDs*.

Morphology and architecture of low- R_{SI} *BSDs*

Low- R_{SI} *BSD6* consists of distributary channel, mouth bar and levée deposits (Fig. 11). Levée deposits are thin at <0.3 m, and the *BSD* is 50 to 200 m wide, which is five to ten times wider than the distributary channel. The bar finger and the distributary channel in *BSD6* are both

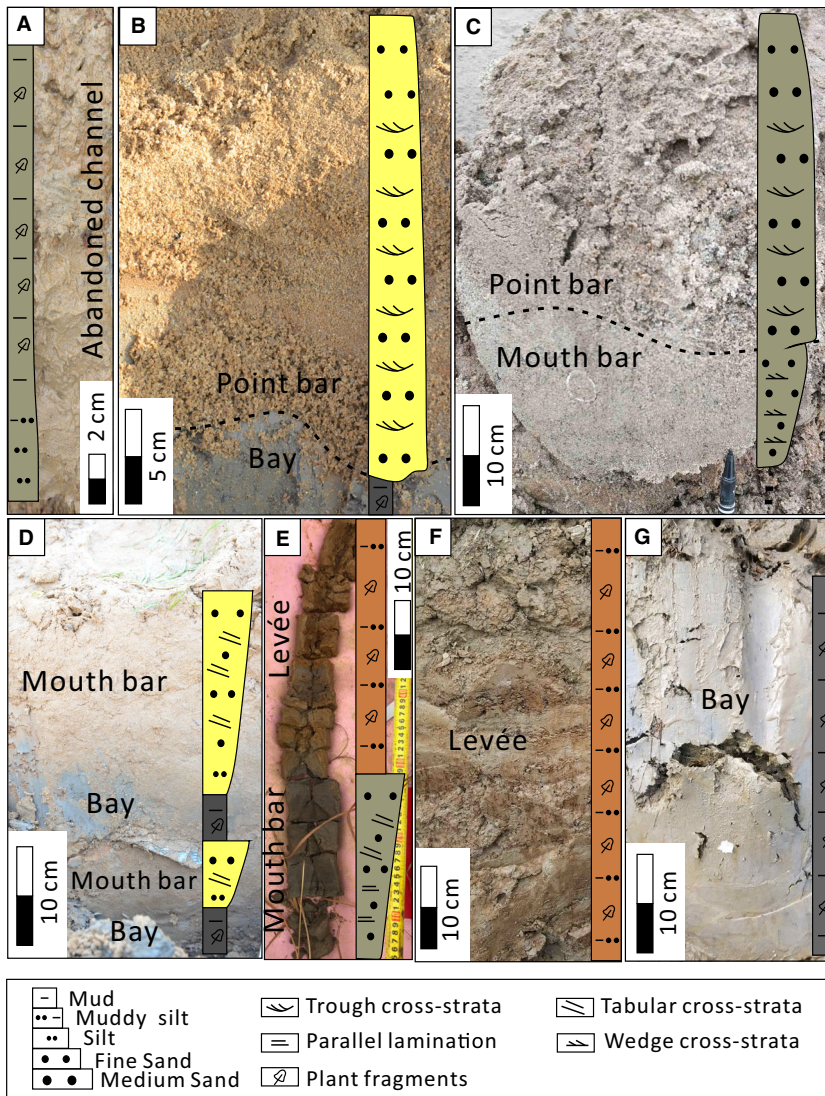


Fig. 10. Photographs and stratigraphic sections of typical facies of abandoned channels (A), point bars (B) and (C); mouth bars (C) to (E), levées (E) and (F), and an inter-distributary bays (G).

sinuous with SI values of 1.22 and 1.20, respectively (Table 1).

The distributary channel incises the central part of the *BSD* in straight sections, and the concave inner bar margin at the bends (Fig. 11). Consequently, the wing-shaped mouth bars are more symmetrical in straight sections, and asymmetrical at bends with a narrower and thinner inner margin wing. The thickest mouth bar deposits occur at the outer bank of distributary channels. The lower elevation of the inner bank is also visible in landform photographs (Fig. 13).

Morphology and architecture of high- R_{SI} *BSDs*

High- R_{SI} *BSDs* consist of distributary channel, mouth bar, levée and point bar deposits. Point

bars occur at the inner banks of distributary channels and are unique for the high- R_{SI} *BSDs*. The distributary channel is 10 to 30 m wide, and the point bars are considerably wider at 30 to 150 m (Fig. 12). *BSD5* is 100 to 300 m wide, which is also five to ten times wider than the distributary channel, but only two to four times wider than the combined width of the distributary channel and point bar deposits. Levées are considerably thicker compared to *BSD5* and approach the thickness of the mouth bars at >0.5 m thick.

BSD5 and the distributary channel have SI values of 1.40 and 1.72, respectively, which are considered meandering. The distributary channel incises the centre of the *BSD* in straight sections, but the incision location varies at bends (Fig. 12). At upstream bends, the distributary channel

Table 2. Characteristics of sedimentary facies.

Facies	Lithological characteristics	Morphology and location
Distributary channel	Brown with a lag of medium sand at the base of active channels; silty sand and dark mud with plant fragments in abandoned channels	Incision topography; contains flowing or standing water
Point bar	Brown or grey with medium and fine sand; fining-upward; wedge to trough cross-strata; scoured base	Crescent-shaped scroll bars at the inner bank
Mouth bar	Grey medium and fine sand; coarsening-upward; tabular strata or planar lamination	Flat base and convex-up top
Levéé	Brown silty mud and some silty sand; fining-upward; plant roots	Overlay other deposits; at channel banks
Inter-distributary bay	Dark mud with plant fragments	Low terrain; contains standing lake water

incises the outer convex margin of the *BSD*. Consequently, the main bar finger occurs along the inner bank, and point bar deposits occur in the central part of the *BSD* (Section C–C' in Fig. 12). At midstream channel bends, the distributary channel incises the central part of *BSD*, and point bar deposits occur at the outer margin of the *BSD* (Section B–B' in Fig. 12). At downstream channel bends, the distributary channel incises the concave inner margin of the *BSD*, and the *BSD* deposits occur at the outer bank with a smaller volume of point bar deposits or without point bars (Section A–A' in Fig. 12). As a result, the inner bank has a higher elevation than the outer bank in the upstream locations (Fig. 14A),

and gradually changes to be lower than the outer bank downstream (Fig. 14B and C). The width and thickness of the point bars decrease downstream, from 200 to 0 m and 1.3 to 0 m, respectively, and point bars are not developed at the most downstream channel bends.

BENDING PROCESSES OF SIMULATED *BSDS*

The simulated *BSDs* have similar architectural characteristics as the modern low- R_{SI} *BSDs*, including $R_{SI} < 1$, incision location of distributary channels, and the *BSD* to distributary

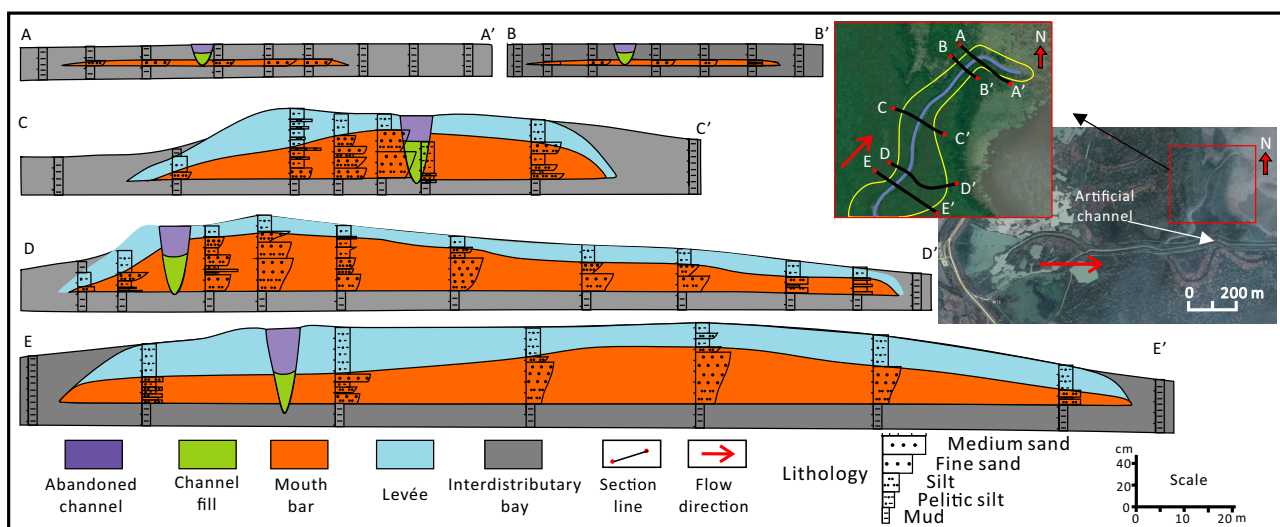


Fig. 11. Architecture and facies distribution of a low sinuosity index (low- R_{SI}) bar finger *BSD6*. Locations of the five cross-sections are indicated by A–A', B–B', C–C', D–D' and E–E' on the insert maps.

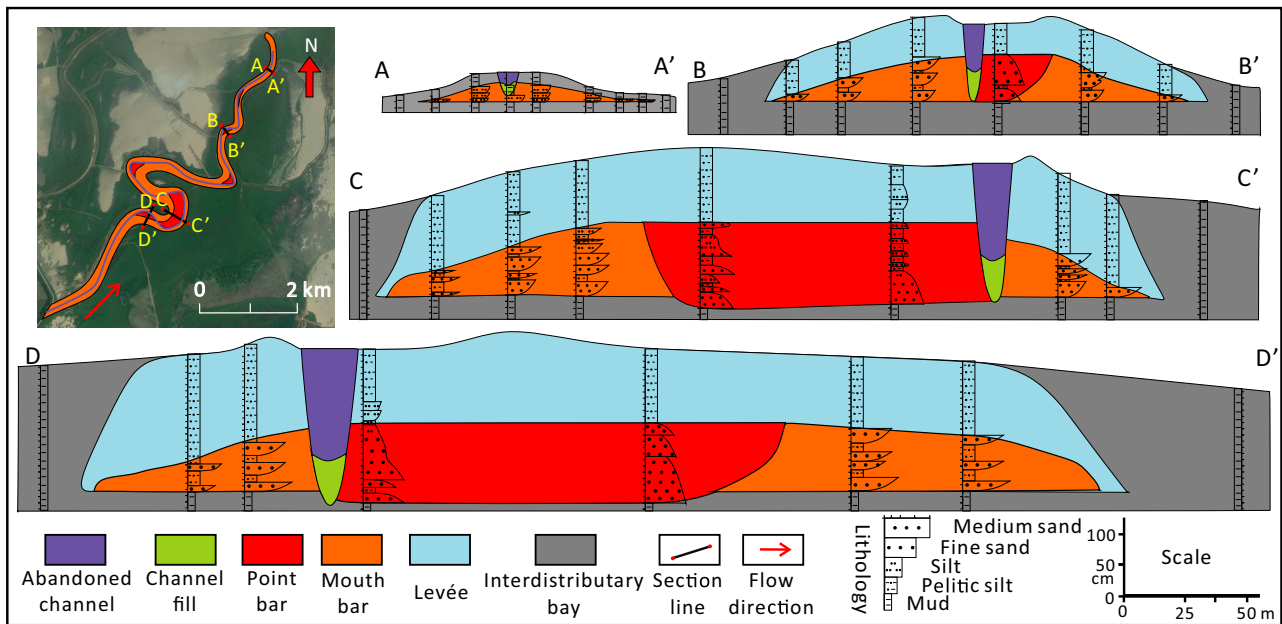


Fig. 12. Architecture and facies distribution of a high sinuosity index (high- R_{SI}) bar finger *BSD5*. Locations of the four cross-sections are indicated by A–A', B–B', C–C' and D–D' on the insert map.

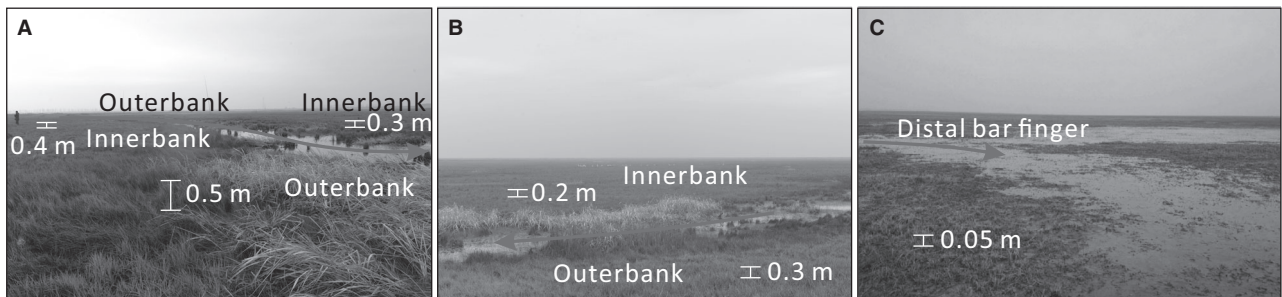


Fig. 13. Photographs of typical landforms of a low sinuosity index (low- R_{SI}) bar finger *BSD6*. Decreasing *Cyperaceae* heights indicate that the elevation of banks decreases downstream from (A) to (C). Arrows point downstream. The *Cyperaceae* height is marked in the photographs.

channel width ratio (Fig. 15). SI_d values in simulations S1 to S3 are all <1.2 , but some distributary channels in simulation S4 have $SI_d >1.2$. The simulation setup did not allow for distributary channel migration, and thus no point bar developed.

The simulations indicate two types of *BSD* bending mechanisms. The first mechanism, also described by Edmonds & Slingerland (2010), results in numerous enclosed bays (Simulation S4, Fig. 15D), and is linked to a high cohesion of fine sediment. An initial channel curvature

creates an asymmetrical mouth bar with a steeper bed slope and more offshore accommodation to one side. More water and sediment are transported there and the accommodation is filled by a curved mouth bar. A bend is created when this branch of the channel is abandoned in favour of the other bifurcated branch of the distributary, which now has a steeper gradient. An enclosed bay forms if sedimentation closes the gap between the mouth bar and the shoreline.

The second mechanism also involves asymmetrical bifurcations (Fig. 16), but results in

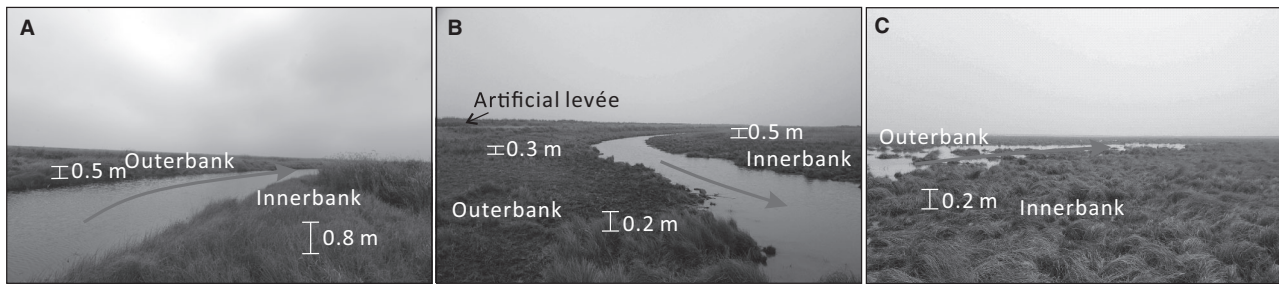


Fig. 14. Photographs of typical landforms of a high sinuosity index (high- R_{SI}) bar finger *BSD5*. Decreasing Cyperaceae heights indicate that the elevation of banks decreases downstream (A) to (C). Inner bank has a higher elevation than outer bank except for lower elevation over point bars. Arrows point downstream. The Cyperaceae height is marked in the photographs.

very few enclosed bays (Simulations S1–S3, Fig. 15A to C). In simulation S3, in the central *BSD* (Fig. 16A) the distributary channel was initially straight and in the centre of the *BSD* (Fig. 16E). When a mouth bar formed, the distributary channel bifurcated (Fig. 16B and F). An asymmetrical bifurcation led the majority of discharge into the right distributary, and the left distributary was gradually abandoned (Fig. 16C and G). This right distributary eroded the right margin of the mouth bar and turned right (Fig. 16C and I). When a new mouth bar formed as the channel extended almost parallel to the shoreline, the discharge was concentrated at the left side of that mouth bar (Fig. 16G). The distributary stopped turning right, and began to erode the left margin of the new mouth bar and turn left (Fig. 16D, H and J). Successively, the distributary channel extended sinuously downstream (Fig. 15C). Similar bending processes occurred in simulations S1 and S2 (Figs 15A, 15B and 17).

DISCUSSION

Bending mechanisms and point bar formation in high- R_{SI} *BSDs*

Since the simulations were not set up to produce point bars, below field and satellite data are used to discuss the bending mechanisms and point bar formation. A point bar is a typical product of lateral channel migration and develops at the inner bank (Leopold & Langbein, 1966; Ikeda, 1989; Smith *et al.*, 2011; Ghinassi *et al.*, 2013, 2016; Ghinassi & Ielpi, 2015; Schuurman *et al.*, 2016). Lateral channel migration is

the result of the secondary flow (Dietrich *et al.*, 1979; Johannesson & Parker, 1989) that is driven by centrifugal force, and arises from the inability of the lateral pressure gradient, associated with the lateral slope of the free surface, to balance the effective centrifugal force (Solari *et al.*, 2002). Lateral migration can be identified from the concave scroll bar morphology (Nanson, 1980; Schuurman *et al.*, 2016; Strick *et al.*, 2018) that forms a curvilinear ridge to the side of the channel and is more or less parallel with the channel (Smith, 1974; Church & Jones, 1982). The concave scroll bar morphology is commonly seen in modern high- R_{SI} *BSDs*, such as in the Ganjiang Delta and Athabasca Delta, but not in low- R_{SI} *BSDs* (Fig. 1).

Based on the distribution of point bars, visible scroll bar morphology and the position of distributary channels, the morphology of initial distributary channels prior to lateral migration and point bar formation were reconstructed for ten high- R_{SI} *BSDs* (see green dashed lines in *BSD4*, *BSD5* and *BSD10* in Fig. 18). These initial distributary channels have similar R_{SI} values, and incise concave inner bar margins in channel bends, similar to the distributary channels in low- R_{SI} *BSDs* (Figs 9 and 11). These similarities suggest that the meandering distributary channels in high- R_{SI} *BSDs* likely initially started as sinuous channels. This conclusion is further supported by that the point bars are missing in the new-growth ends of the high- R_{SI} *BSDs* and distributary channels are still sinuous (Fig. 12). Successive lateral distributary channel migration resulted in increased channel sinuosity, but had no influence on the sinuosity of *BSDs*, as the channels did not migrate beyond the original boundaries

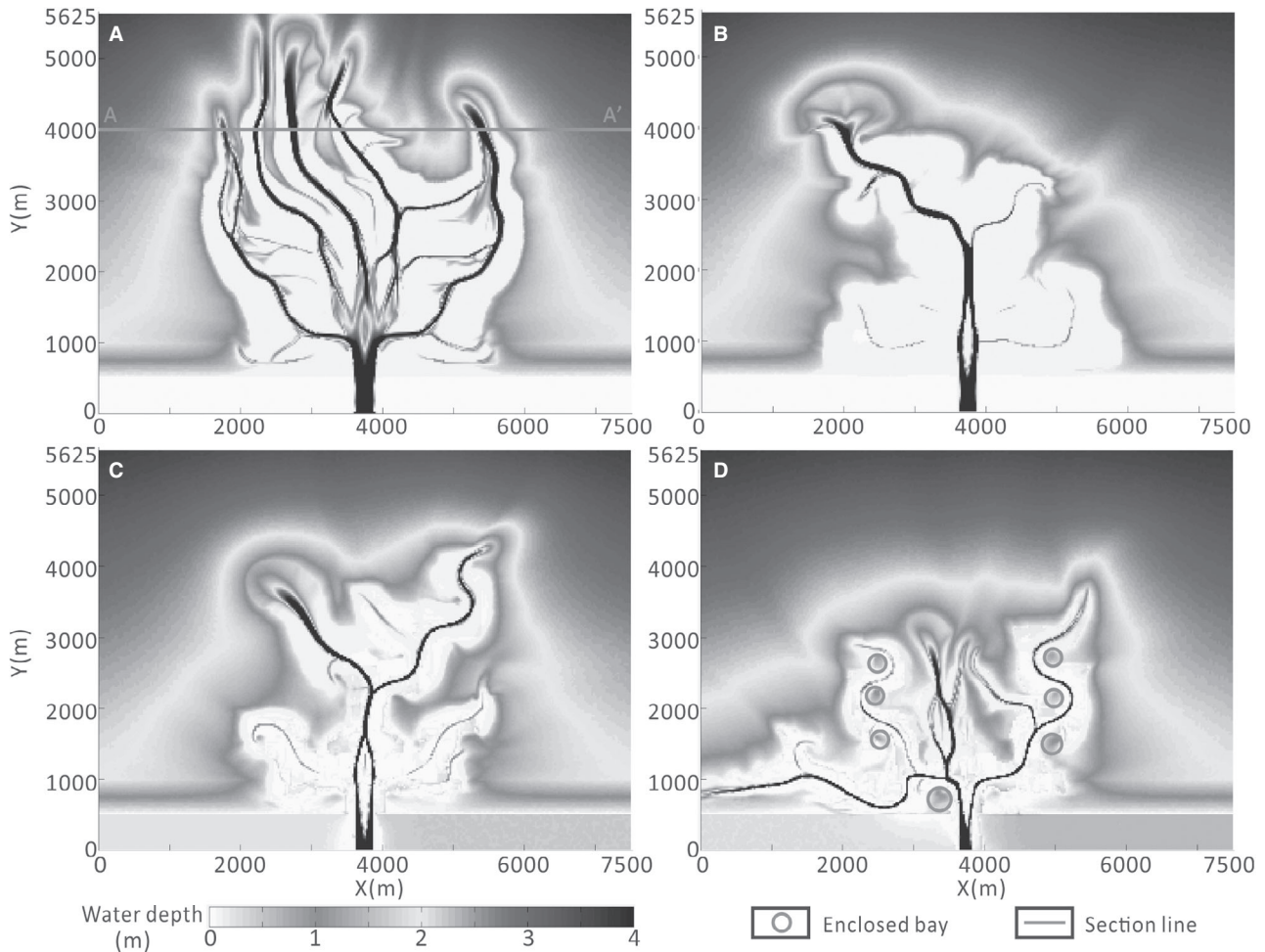


Fig. 15. Map views of simulations S1 to S4 with different sediment cohesion values. The *critical shear stress for erosion of the cohesive sediment fraction* [$\tau_{ce}(c)$] values in the four models are; 0.25 (A), 1.0 (B), 2.0 (C) and 3.25 (D) N/m^2 , respectively. Enclosed bays developed only in simulation S4 (D).

of their *BSDs*, i.e. beyond the lateral extent of the mouth bar deposits that the distributaries are eroded into (Fig. 12). This study thus suggests that both low- R_{SI} and high- R_{SI} *BSDs* initially extend basinward sinuously. As a secondary process, the distributary channels in the high- R_{SI} *BSDs* develop higher sinuosity by lateral migration and point bar formation, whereas *BSDs* retain their initial sinuosity, but develop thicker levées. Bends in the channels expanded by lateral migration coincide with the pre-existing bends in the bar-finger. Lateral migration towards the convex outer bend results in distributary channel incision near the outer bends in proximal (older) *BSDs* with wide point bar deposits due to the longer migration duration (Figs 12 and 18). In contrast, near the

new-growth ends of *BSDs*, where point bars are narrow or missing, the distributary channels incise in the centre or near the inner bend (Fig. 18).

The bending mechanism of initial distributary channels in *BSDs* needs further research. This work compares to the fluvial channel bending mechanisms that have been a subject of continued research. A key mechanism by which a straight channel evolves into a meandering channel is the formation of alternate bars, and consequent deflection of flow in the presence of stable river banks (e.g. Ikeda, 1981; Parker *et al.*, 1982; Blondeaux & Seminara, 1985; Rhoads & Welford, 1991; Kleinbans, 2010; Luchi *et al.*, 2011). Since alternate bars have not been observed in this dataset, nor formed in

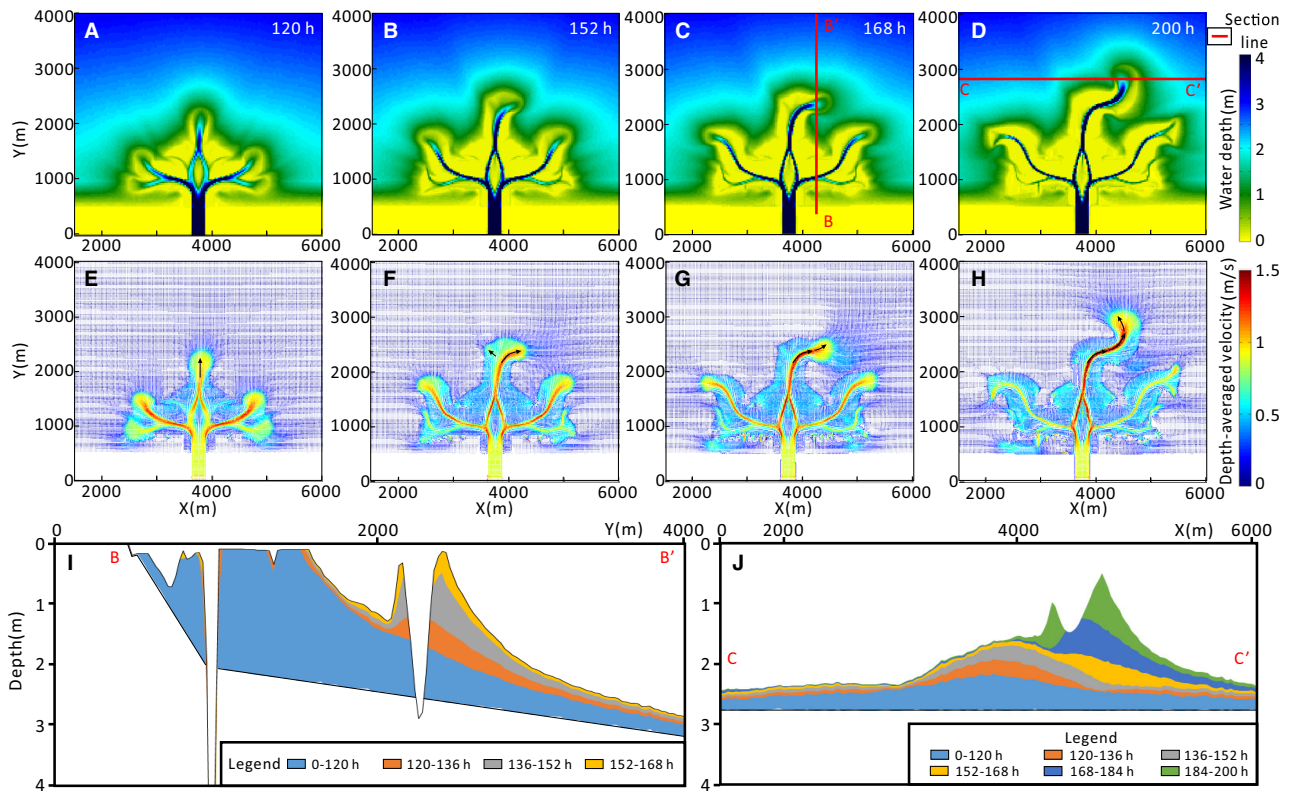


Fig. 16. Map views of four critical time steps (A) to (D) in simulation S3, and corresponding maps of depth-averaged velocity (E) to (H). Flow parallel (I) and perpendicular (J) sediment cross-sections. The locations of cross-sections are shown in (C) and (D).

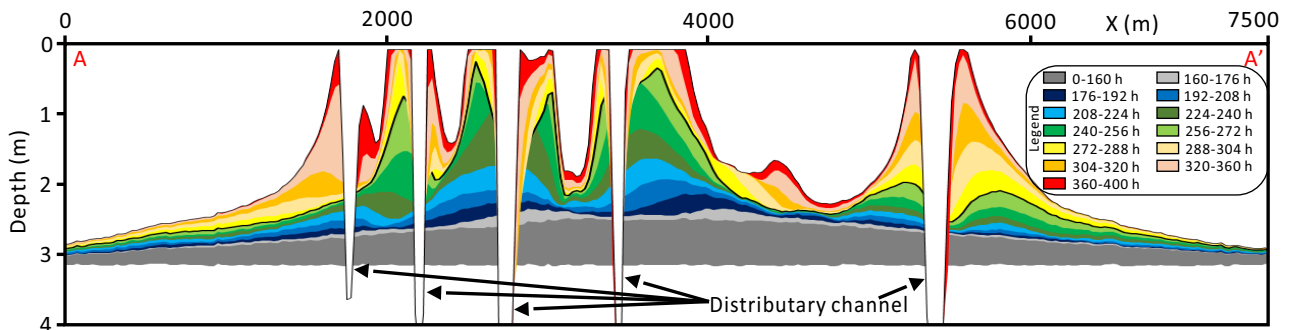


Fig. 17. Sediment cross-section from simulation S1. The location of the cross-section is shown in Fig. 15A.

simulations (Figs 11, 12 and 15), the formation of alternate bars does not seem to be the cause of sinuous distributary channels in *BSDs* (Fig. 1). An alternative mechanism suggests that spatial irregularities of initial substrate, upon which the channel forms, cause variances in flow resistance and lead to an initial meandering

pattern (Lazarus & Constantine, 2013). This mechanism seems a more likely explanation, as distributary channels generate their own spatial irregularities through deposition of mouth bars in the distributary mouth. Simulations demonstrate (Fig. 16E to H) how flow is deflected by the perturbation of mouth bars in *BSDs*.

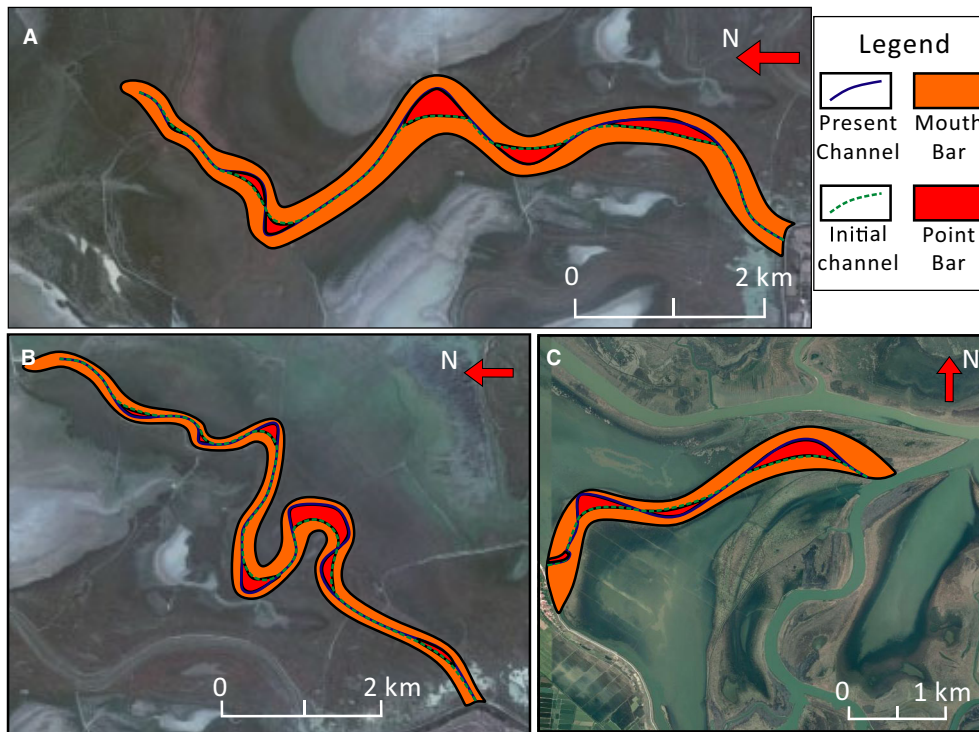


Fig. 18. Satellite images of *high sinuosity ratio* (high- R_{S1}) bar fingers where the initial distributary channel sinuosity was restored using point bar distributions (see text): *BSD4* (A), *BSD5* (B) and *BSD10* (C).

The authors thus suggest that the transition from low- R_{S1} to high- R_{S1} *BSDs* may depend on the slight differences in sinuosity in the initial low- R_{S1} *BSDs*, as also indicated by the trend lines in Fig. 9. The centrifugal force increases with the increase of inertia and curvature (Leopold & Wolman, 1960; Seminara & Tubino, 1989; Stoesser *et al.*, 2010), and bends with larger initial sinuosity should have higher migration rates (Sylvester *et al.*, 2019). Initial sinuosity in the channel is inherited from the sinuosity generated in the bar finger from mouth bars because the channel by default had to follow the bar finger. Higher-sinuosity low- R_{S1} *BSDs* thus seem more likely to turn into high- R_{S1} *BSDs*, and perhaps this is why low- R_{S1} *BSDs* with channel sinuosity of >1.2 are rare (Fig. 9). These other factors of centrifugal force and substrate irregularities would exacerbate this initial sinuosity. In the initially higher-sinuosity bends, distributary channel would have more inherited sinuosity and thus generate more centrifugal force.

High- R_{S1} *BSDs* develop thick levées that according to the trash dates indicate longer accretion times than the thin levées in low- R_{S1}

BSDs (Figs 11 and 12), such as 40 versus 10 years in some examples. This, together with the lack of meandering near the new-growth ends of the *BSDs*, suggests that duration (time) seems a second formation condition of high- R_{S1} *BSDs*.

The role of cohesion in bending of *BSDs*

Cohesion determines channel bank strength and channel morphology, where high cohesion banks promote meandering in rivers, rather than braided channel morphology (Ferguson, 1987; Nanson & Croke, 1992; Paola, 2001; Tal & Paola, 2007; Braudrick *et al.*, 2009; Howard, 2009). However, the reduction of bank erodibility due to cohesion may also inhibit channel migration (Peakall *et al.*, 2007). It has been also suggested that high cohesion reduces secondary lateral migration of distributary channels (Edmonds & Slingerland, 2010).

Cohesion clearly affected the bending process of *BSDs*, as simulations with high sediment cohesion (S4) developed enclosed bays and simulations with moderate cohesion (S1–S3) did not (Fig. 15). The initial bending of *BSDs* is

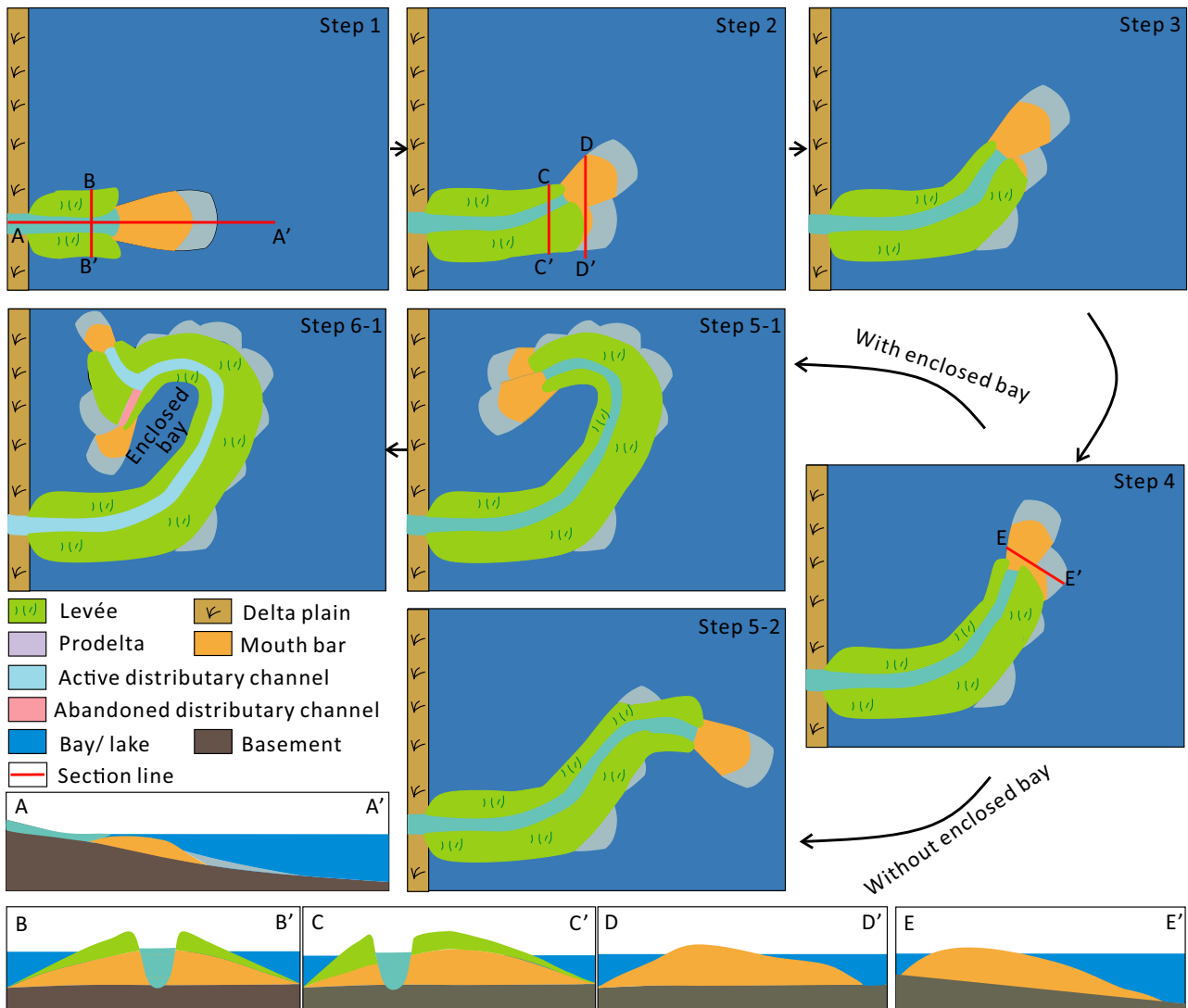


Fig. 19. Schematic diagrams of initial bar finger bending processes that create sinuosity and lead to bending with creation of enclosed bays (5-1; 6-1) or without the enclosed bays (5-2).

similar in both cases until *BSDs* are almost parallel to the shoreline (Steps 1–4 in Fig. 19). In high-cohesion *BSDs* (S4), bank strength exceeds the centrifugal force of water flow, the *BSD* continues to bend upstream and an enclosed bay forms at the inner-bend (Step 5-1 in Fig. 19). For low-cohesion *BSDs* (Simulations S1–S3), bank strength is not enough to resist downstream flow, and the distributary channel bends downstream without forming an enclosed bay (Step 5-2 in Fig. 19). In these simulations higher sediment cohesion increases sinuosity of the initial bends, and promotes the formation of enclosed bays. The number of enclosed bays has a

positive linear relationship with the critical shear stress for erosion $\tau_{ce}(c)$, where higher $\tau_{ce}(c)$ reflects higher sediment cohesion (Fig. 20) (see also Edmonds & Slingerland, 2010). Numerical simulations of Edmonds & Slingerland (2010) and of this study, both show $\tau_{ce}(c)$ values of $>1.0 \text{ N m}^{-2}$ to form enclosed bays. Field observation (Fig. 1) indicates that cohesion is still not sufficient to generate enclosed bays in most natural *BSDs*, even with the added bank cohesion provided by roots.

Numerical simulations from Edmonds & Slingerland (2010) and of this study (Fig. 15) further show that high sediment cohesion

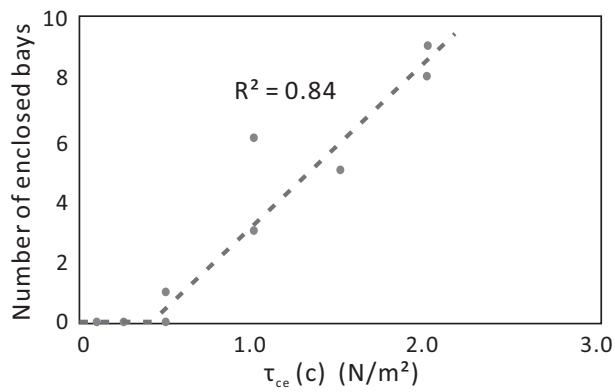


Fig. 20. Relationship between the number of enclosed bays and sediment cohesion. $\tau_{ce}(c)$ is defined as the critical shear for erosion of the cohesive sediment fraction (Edmonds & Slingerland, 2010). The sediment is more cohesive as $\tau_{ce}(c)$ increases. When $\tau_{ce}(c)$ is <0.5 N/m^2 , enclosed bays cannot develop under the depositional conditions in Edmonds & Slingerland (2010).

increases *BSD* sinuosity. Our field data agree with this result in that cohesion and proportion of fine sediments in *BSD10* is lower than that in *BSD4* and *BSD5*, and the sinuosity of *BSD10* is lower (Fig. 18).

Effect of water depth on sinuosity and causal mechanisms

Differences in modern *BDDs* and *BSDs* and their distributary channel sinuosity (Table 1; Fig. 8) imply that water depth may have an important influence on the sinuosity of distributary channels and bar fingers in digitate deltas. Water depth controls the hydrodynamics of outflows, as deep channel outlets promote ‘inertia-dominated effluents’ with a high outflow velocity, a constant low spreading angle, weak streamwise velocity decay, and little bedload transport (Wright, 1977; Postma, 1990; Falcini & Jerolmack, 2010). Shallow channel outlets have

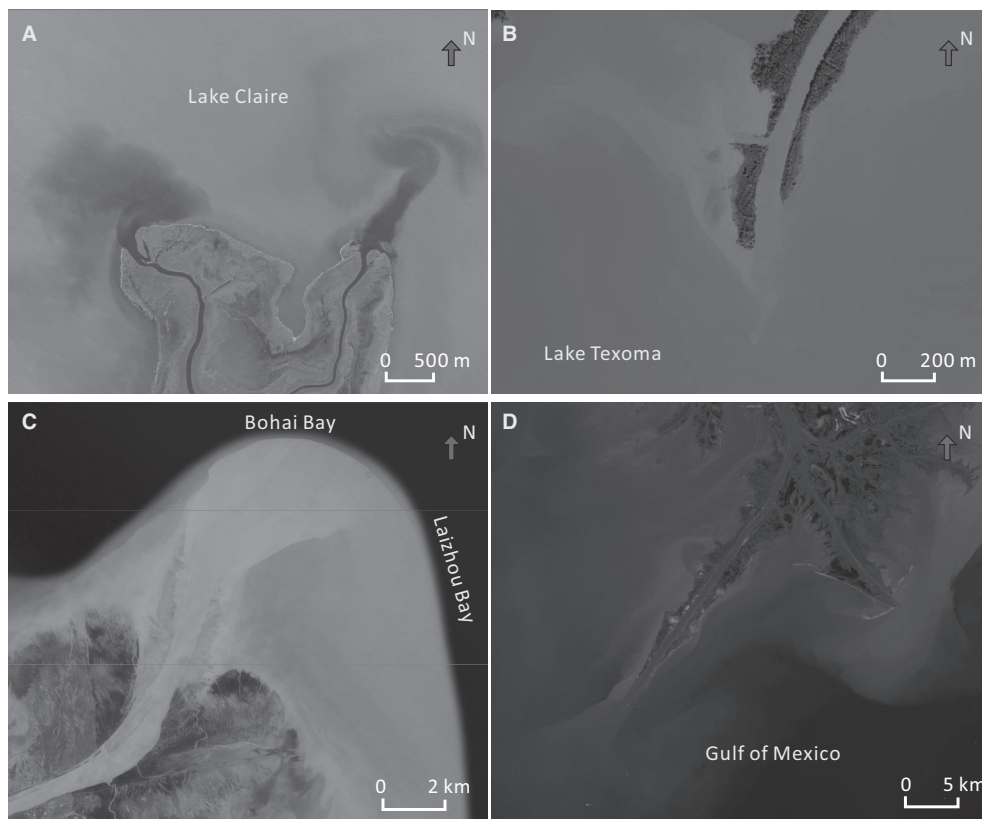


Fig. 21. Jet morphology in distal bar fingers shallow-water (A) and (B) and deep-water (C) and (D) digitate deltas. Meandering jets the Claire Delta (A) and in Lake Texoma (B). Straight jets in the Yellow River Delta (C) and the Mississippi Delta (D).

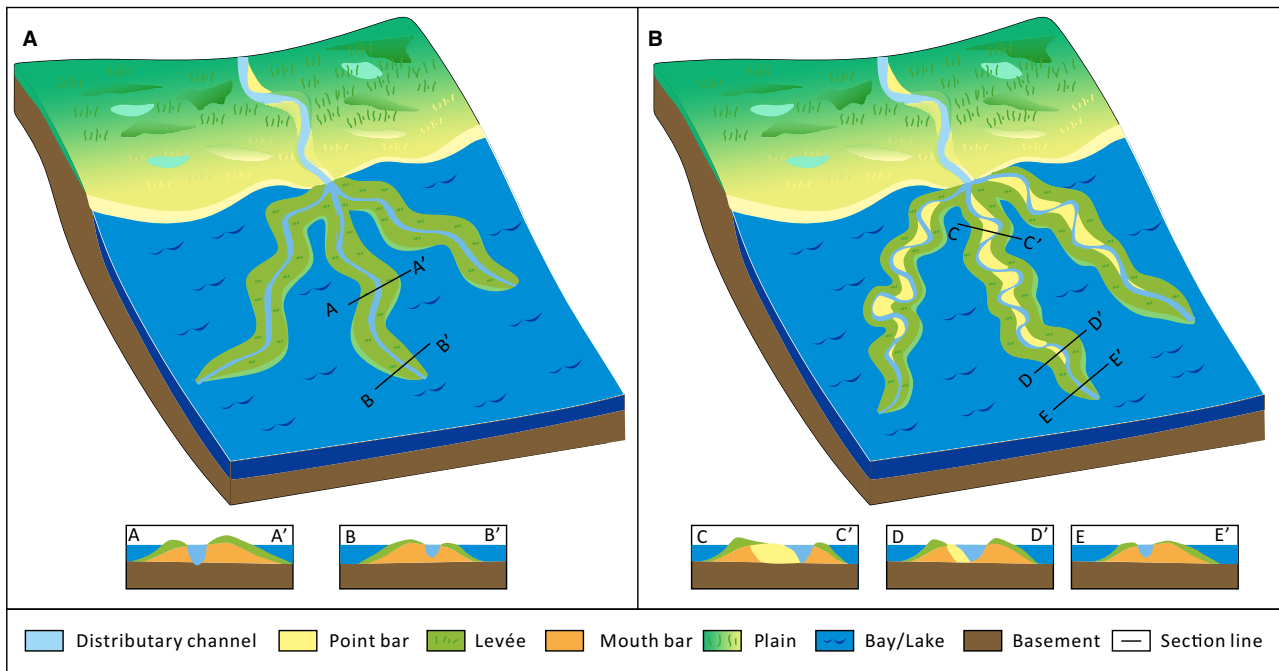


Fig. 22. Facies models for two types of shallow-water bar fingers: (A) low (low- R_{SI}) and (B) high (high- R_{SI}) sinuosity ratio bar fingers.

‘friction-dominated effluents’, characterized by a more moderate outflow jet velocity and a rapid lateral expansion and deceleration (Wright, 1977; Postma, 1990; Falcini & Jerolmack, 2010). Therefore, the shallow channel outlets promote rapid deposition of mouth bars that then divert flow around the mouth bar, resulting in the formation of sinuous *BSDs* with sinuous distributary channels. In contrast, the inertia-dominated effluents continue over a central mouth bar until the elevation of the mouth bar is higher than the bottom of the distributary channel in the *BDD* outlet, resulting in the formation of straight *BDDs*.

Furthermore, in shallow-water deltas the outflow jet meanders, as seen in modern (Fig. 21A and B), simulated (Fig. 16) and experimental *BSDs* (Giger *et al.*, 1991; Dracos *et al.*, 1992; Socolofsky & Jirka, 2004; Rowland *et al.*, 2009). In comparison, the jet is relatively straight in *BDDs* (Fig. 21C and D). Jet starts to meander around its centreplane beyond a distance of approximately ten times the depth of the receiving water body (Dracos *et al.*, 1992). Therefore, jet meandering is more common in shallow outlets. Jet meandering increases lateral sediment transport (Mariotti *et al.*, 2013) that in turn supports the sinuosity of *BSDs*.

Lazarus & Constantine (2013) explain channel sinuosity by the ratio of the flow-resistance variance to the slope. Channel sinuosity positively scales with this ratio, which relates to the Froude number. This may help to explain the higher distributary channel sinuosity in *BSDs*. In *BSDs*, higher flow-resistance and lower gradient with lower Froude number promotes formation of sinuous distributary channels, compared to *BDDs*. Thus, there is likely a tendency of distributary channels to be more sinuous in shallower-water basins.

Effect of bending processes on the architecture of *BSDs*

The architecture of the low- R_{SI} and high- R_{SI} *BSDs* is distinct (Figs 11, 12 and 22) due to the secondary lateral channel migration and formation of point bars in the high- R_{SI} *BSDs*. These processes determine the differences in sediment type (presence or absence of point bar deposits), as well as the location of channel incision in *BSDs*. The initial incision location in the concave inner bar margins is replaced by incision in the outer convex margin in the bends where lateral migration and point bars develop in high-

R_{SI} BSDs (Fig. 22). The initial incision location is however preserved in low- R_{SI} BSDs, and in the new-growth ends of high- R_{SI} BSDs.

The downstream decrease in BSD width, sinuosity and channel incision depth in both types of BSDs may perhaps be explained by an increase in water depth (Edmonds *et al.*, 2011). However, the BSD thickness also decreases downstream, suggesting a decrease in sediment supply. This is similar to a mechanism proposed for the downstream decrease in river sinuosity near the coast (Gouw & Autin, 2008) due to sequestration of sand by point bar growth that starves the downstream meanders (Blum *et al.*, 2013). Since the reduction occurs both in low- R_{SI} and high- R_{SI} BSDs, compared to this mechanism, the short duration of BSD evolution near the new-growth ends seems a more important cause.

Implications for land building plans

Recently, a land-building plan was proposed for the Mississippi Delta that creates artificial deltas by diversions into shallow-water bays (DeLaune *et al.*, 2003; Day *et al.*, 2007; Kim *et al.*, 2009b; Rego *et al.*, 2010; Paola *et al.*, 2011; Nittrouer *et al.*, 2012; Falcini *et al.*, 2012), aiming to resolve severe coastline retreat and loss of deltaic wetlands (Britsch & Dunbar, 1993; Day *et al.*, 2000; Georgiou *et al.*, 2005; Penland *et al.*, 2005; Syvitski & Saito, 2007; Campanella, 2008; Törnqvist *et al.*, 2008; Syvitski *et al.*, 2009; Fagherazzi *et al.*, 2015). The current plan adopts the lobate Wax Lake Delta as a prototype to predict how the artificial deltas grow (Kim *et al.*, 2009a). However, the natural Balize lobe of the Mississippi Delta is a digitate delta with BDDs (Fagherazzi *et al.*, 2015). It seems that a diversion of flow into shallow bays would thus rather create BSDs. Results of this work show how different BSDs extend into the basin and evolve, and thus how they are likely to build new land. It shows that both low- R_{SI} and high- R_{SI} BSDs generate narrow fingers of land with land widths of five to ten times of the distributary channel width, and that lateral distributary channel migration and point bar formation does not increase BSD width, but rather reworks the mouth bar deposits.

CONCLUSIONS

This paper shows that bar fingers in digitate deep-water (BDDs) and shallow-water deltas (BSDs)

differ in that BDDs and their distributary channels strongly tend to be straight and BSDs and their distributary channels strongly tend to be sinuous. These differences are here assigned to the effect of water depth on outflow hydraulics, where shallow water depths promote effluent friction, rapid aggradation of mouth bars that then divert flow around the mouth bars, resulting in sinuous BSDs and distributary channels. The inertia-dominated deep-water effluents continue over a central mouth bar until the elevation of the mouth bar is higher than the bottom of the distributary channel in the BDD outlet, resulting in the formation of straight BDDs. These effects are further strengthened by the meandering of the shallow water jet that increases lateral sediment transport, and by the higher flow resistance and lower gradient of the shallow-water outflows. This study further shows that BSDs develop sinuous or meandering distributary channels as a function of slight initial differences in channel sinuosity. Lateral channel migration and point bar formation occur as a secondary process that does not change the shape or width of the BSDs. However, differences in distributary channel morphology have a strong effect on BSD sediment type, architecture and morphology. Sediment cohesion is another important control on BSD bending processes, because high cohesion BSDs form enclosed bays due to the fact that their bank strength exceeds the centrifugal force of water flow. This work provides insights into natural and artificial shallow-water digitate delta growth and provides new detailed facies models for BSDs.

ACKNOWLEDGEMENTS

The work presented in the paper was financially supported by the National Natural Science Foundation of China (No. 41772101) and China Scholarship Council. We thank A. P. Burpee for help with the Delft3D simulations. We thank reviewers David Went, Amy Gough, John Holbrook, and other anonymous reviewers, and the Associate Editor Massimiliano Ghinassi for constructive reviews that significantly improved the manuscript.

DATA AVAILABILITY STATEMENT

Data are openly available in a public repository that issues datasets with <https://doi.org/10.17632/hcykmcj2x9.1>.

REFERENCES

- Avery, S.T. and Tebbs, E.J. (2018) Lake Turkana, major Omo River developments, associated hydrological cycle change and consequent lake physical and ecological change. *J. Great Lakes Res.*, **44**(6), 1164–1182.
- Baar, A.W., Boechat Albernaz, M., van Dijk, W.M. and Kleinhans, M.G. (2019) Critical dependence of morphodynamic models of fluvial and tidal systems on empirical downslope sediment transport. *Nat. Commun.*, **10**(1), 1–12.
- Bagnold, R.A. (1966) An approach to the sediment transport problem from general physics. USGS professional paper, 422-I, U.S. Government Printing Office, Washington, D. C.
- Bates, C.C. (1953) Rational theory of delta formation. *AAPG Bull.*, **37**, 2119–2162.
- Bernard, H.A. (1965) A resume of river delta types: Abstract. *AAPG Bull.*, 49 pp.
- Blondeaux, P. and Seminara, G. (1985) A unified bar-bend theory of river meanders. *J. Fluid Mech.*, **157**, 449–470.
- Blum, M., Martin, J., Milliken, K. and Garvin, M. (2013) Paleovalley systems: insights from quaternary analogs and experiments. *Earth Sci. Rev.*, **116**, 128–169.
- Braudrick, C.A., Dietrich, W.E., Leverich, G.T. and Sklar, L.S. (2009) Experimental evidence for the conditions necessary to sustain meandering in coarse-bedded rivers. *Proc. Natl. Acad. Sci. USA*, **106**(40), 16936–16941.
- Brice, J.C. and Blodgett, J.C. (1978) Countermeasures for hydraulic problems at bridges, Volume 1 Analysis and Assessment: Federal Highway Administration Report No. FHWA-RD-78-162, September 1978 Final Report, 169 p.
- Bridge, J.S. (2003) *Rivers and Floodplains: Forms, Processes, and Sedimentary Record*. Blackwell, Malden, MA, 152 pp.
- Britsch, L.D. and Dunbar, J.B. (1993) Land loss rates: Louisiana coastal plain. *J. Coastal Res.*, **9**, 324–338.
- Burpee, A.P., Slingerland, R.L., Edmonds, D.A., Parsons, D., Best, J., Cederberg, J., McGuffin, A., Caldwell, R., Nijhuis, A. and Royce, J. (2015) Grain-size controls on the morphology and internal geometry of river-dominated deltas. *J. Sed. Res.*, **85**, 699–714.
- Caldwell, R.L. and Edmonds, D.A. (2014) The effects of sediment properties on deltaic processes and morphologies: a numerical modeling study. *J. Geophys. Res. Earth Surf.*, **119**, 961–982.
- Caldwell, R.L., Edmonds, D.A., Baumgardner, S., Paola, C., Roy, S. and Nienhuis, J.H. (2019) A global delta dataset and the environmental variables that predict delta formation on marine coastlines. *Earth Surf. Dynam.*, **7**(3), 773–787.
- Campanella, R. (2008) *Bienville's Dilemma: A Historical Geography of New Orleans*. University of Lafayette, Lafayette, 429 pp.
- Church, M. and Jones, D. (1982) Channel bars in gravel-bed rivers. In: *Gravel Bed Rivers* (Eds Hey, R.D., Bathurst, J.C. and Thorne, C.R.), pp. 291–338. Wiley, Chichester.
- Day, J.W., Boesch, D.F., Clairain, E.J., Kemp, G.P., Laska, S.B., Mitsch, W.J., Orth, K., Mashriqui, H., Reed, D.J., Shabman, L., Simenstad, C.A., Streever, B.J., Twilley, R.R., Watson, C.C., Wells, J.T. and Whigham, D.F. (2007) Restoration of the mississippi delta: lessons from hurricanes katrina and rita. *Science*, **315**, 1679–1684.
- Day, J.W., Britsch, L.D., Hawes, S.R., Shaffer, G.P., Reed, D.J. and Cahoon, D. (2000) Pattern and process of land loss in the Mississippi Delta: a spatial and temporal analysis of wetland habitat change. *Estuaries*, **23**, 425–438.
- DeLaune, R.D., Jugsujinda, A., Peterson, G.W. and Patrick, W.H. (2003) Impact of Mississippi River freshwater reintroduction on enhancing marsh accretionary processes in a Louisiana estuary. *Estuarine Coastal Shelf Sci.*, **58**, 653–662.
- Dietrich, W.E., Smith, J.D. and Dunne, T. (1979) Flow and sediment transport in a sand bedded meander. *J. Geol.*, **87**, 305–315.
- Dissanayake, D.M.P.K., Roelvink, J.A. and Van der Wegen, M. (2009) Modelled channel patterns in a schematized tidal inlet. *Coastal Eng.*, **56**(11–12), 1069–1083.
- Donaldson, C.A. (1974) Pennsylvanian sedimentation of central appalachians. *Spec. Pap. Geol. Soc. Am.*, **148**, 47–48.
- Dracos, T., Giger, M. and Jirka, G.H. (1992) Plane turbulent jets in a bounded fluid layer. *J. Fluid Mech.*, **241**, 587–614.
- Drosou, A., Dimitriadis, P., Lykou, A., Kossieris, P., Tsoukalas, I., Efstratiadis, A. and Mamassis, N. (2015) Assessing and optimising flood control options along the Arachthos river floodplain (Epirus, Greece). In: EGU General Assembly Conference Abstracts, Vol. 17, Session NH1.6:Flood risk and uncertainty, Vienna, Austria, EGU2015-9148-1.
- Duan, D., Hou, J., Liu, Y., Wang, C. and Gao, J. (2014) Quantitative research of fluvial-dominated delta front sedimentary system: a case study of Poyang Lake delta. *Acta Sedimentol. Sin.*, **32**, 270–277.
- Dumars, A.J. (2002) *Distributary mouth bar formation and channel bifurcation in the Wax Lake Delta, Atchafalaya Bay, Louisiana*. Louisiana State University, Baton Rouge, 88 pp.
- Edmonds, D.A., Caldwell, R.L., Brondizio, E.S. and Siani, S.M.O. (2020) Coastal flooding will disproportionately impact people on river deltas. *Nat. Commun.*, **11**(1), 1–8.
- Edmonds, D.A., Shaw, J.B. and Mohrig, D. (2011) Topset-dominated deltas: a new model for river delta stratigraphy. *Geology*, **39**(12), 1175–1178.
- Edmonds, D.A. and Slingerland, R.L. (2010) Significant effect of sediment cohesion on delta morphology. *Nat. Geosci.*, **3**, 105–109.
- Fagherazzi, S., Edmonds, D.A., Nardin, W., Leonardi, N., Canestrelli, A., Falcini, F., Jerolmack, D., Mariotti, G., Rowland, J.C. and Slingerland, R.L. (2015) Dynamics of river mouth deposits. *Rev. Geophys.*, **53**, 642–672.
- Falcini, F. and Jerolmack, D.J. (2010) A potential vorticity theory for the formation of elongate channels in river deltas and lakes. *J. Geophys. Res. Earth Surf.*, **115**, F04038.
- Falcini, F., Khan, N.S., Macelloni, L., Horton, B.P., Lutken, C.B., McKee, K.L., Santoleri, R., Colella, S., Li, C., Volpe, G., D'Emidio, M., Salusti, A. and Jerolmack, D.J. (2012) Linking the historic 2011 Mississippi River flood to coastal wetland sedimentation. *Nat. Geosci.*, **5**, 803–807.
- Feng, W., Wu, S., Zhang, K., Zhao, W. and Jia, F. (2017) Depositional process and sedimentary model of meandering-river shallow delta: insights from numerical simulation and modern deposition. *Acta Geol. Sin.*, **91**, 2047–2064.
- Ferguson, R. (1987) Hydraulic and sedimentary controls of channel pattern. In: *River Channels: Environment and Process* (Ed. Richards, K.), *Inst. Br. Geogr. Spec. Publ.*, **18**, 129–158.
- Fisher, W.L., Brown, L.F., Scott, A.J. and McGowen, J.H. (1969) *Delta Systems in the Exploration for Oil and Gas*. Bureau of Economic Geology, University of Texas, Austin, TX, 78 pp.

- Fisk, H.N.** (1954) Sedimentary framework of the Modern Mississippi Delta. *J. Sediment. Petrol.*, **24**, 76–99.
- Fisk, H.N.** (1955) Sand facies of Recent Mississippi delta deposit. *4th World Petroleum Congress, Rome, Italy*, 377–398.
- Fisk, H.N.** (1961) Bar-finger sands of Mississippi delta. In: *Geometry of Sandstone Bodies* (Eds Peterson, J.A. and Osmond, J.C.), *AAPG, Tulsa, Okla.*, 29–52.
- Galloway, W.E.** (1975) Process framework for describing the morphologic and stratigraphic evolution of deltaic depositional systems. In: *Deltas: Models for Exploration* (Ed. Broussard, M.L.), pp. 87–98. Houston Geological Society, Houston, TX.
- Gao, Z., Zhou, C., Dong, W., Bai, B. and Li, W.** (2016) Sedimentary processes, depositional model and sandbody prediction of lacustrine shallow water delta: a case study of Ganjiang River Delta in Poyang Lake. *Geoscience*, **30**, 341–352.
- Geleynse, N., Storms, J.E.A., Walstra, D.J.R., Jagers, H.R.A., Wang, Z.B. and Stive, M.J.F.** (2011) Controls on river delta formation; insights from numerical modeling. *Earth Planet. Sci. Lett.*, **302**, 217–226.
- Georgiou, I.Y., FitzGerald, D.M. and Stone, G.W.** (2005) The impact of physical processes along the Louisiana coast. *J. Coastal Res.*, **44**, 72–89.
- Ghinassi, M., Billi, P., Libsekal, Y., Papini, M. and Rook, L.** (2013) Inferring fluvial morphodynamics and overbank flow control from 3D outcrop sections of a Pleistocene point bar, Dandiero Basin. *Eritrea. J. Sed. Res.*, **83**(12), 1066–1084.
- Ghinassi, M. and Ielpi, A.** (2015) Stratal architecture and morphodynamics of downstream-migrating fluvial point bars (Jurassic Scalby Formation, UK). *J. Sed. Res.*, **85**(9), 1123–1137.
- Ghinassi, M., Ielpi, A., Aldinucci, M. and Fustic, M.** (2016) Downstream-migrating fluvial point bars in the rock record. *Sed. Geol.*, **334**, 66–96.
- Giger, M., Dracos, T. and Jirka, G.H.** (1991) Entrainment and mixing in plane turbulent jets in shallow water. *J. Hydraul. Res.*, **29**(5), 615–642.
- Gouw, M.J.P. and Autin, W.J.** (2008) Alluvial architecture of the holocene lower mississippi valley (U.S.A.) and a comparison with the rhine-meuse delta (the Netherlands). *Sed. Geol.*, **204**(3–4), 106–121.
- Howard, A.D.** (2009) How to make a meandering river. *Proc. Natl. Acad. Sci. USA*, **106**(41), 17245–17246.
- Hu, C.** (1999) A historical study on the back flows of Water from the Changjiang River to the Poyang Lake at Hukou, Jiangxi. *Acta Geogr. Sin.*, **54**, 79–84.
- Hu, C.H., Qu, H.J., Miao, J.Y., Wang, W.L. and Ma, Q.** (2008) A study on sedimentary microfacies and oil-bearing possibility in Chang 6 oil-bearing formation in the area of Nanniwan. *J. Northwest Univ.*, **38**(6), 994–1000.
- Huang, X., Liu, K., Zou, C., Gui, L., Yuan, X. and Qin, Y.** (2013) Forward stratigraphic modeling of the depositional process and evolution of shallow water deltas in Poyang Lake, Southern China. *Earth Sci. J. China Univ. Geosci.*, **38**, 1005–1013.
- Ikeda, H.** (1989) Sedimentary controls on channel migration and origin of point bars in sand-bedded meandering rivers. *River Meandering*, **12**, 51–68.
- Ikeda, S.** (1981) Self-formed straight channels in sandy beds. *J. Hydraul. Div. Am. Soc. Civ. Eng.*, **107**, 389–406.
- Ikeda, S.** (1982) Lateral bed load transport on side slopes. *J. Hydraul. Div. ASCE*, **108**(11), 1369–1373.
- Jin, Z., Gao, B., Wang, J., Li, Y., Shi, L., Yu, K. and Li, G.** (2017) Two new types of sandbars in channels of the modern Ganjiang Delta, Poyang Lake, China: depositional characteristics and origin. *J. Palaeogeogr.*, **6**(2), 132–143.
- Jin, Z., Li, Y., Gao, B., Song, B., He, Y., Shi, L. and Li, G.** (2011) Depositional model of modern gentle-slope delta: a case study from Ganjiang delta in Poyang Lake. *Acta Sedimentol. Sin.*, **32**(4), 710–723.
- Johannesson, H. and Parker, G.** (1989) Linear theory of river meanders. In: *River Meandering* (Eds Ikeda, S. and Parker, G.), *Am. Geophys. Union Water Res. Monogr.*, **12**, 181–213.
- Kim, W., Dai, A., Muto, T. and Parker, G.** (2009a) Delta progradation driven by an advancing sediment source: coupled theory and experiment describing the evolution of elongated deltas. *Water Resour. Res.*, **45**, W06428.
- Kim, W., Mohrig, D., Twilley, R., Paola, C. and Parker, G.** (2009b) Is it feasible to build new land in the Mississippi River delta? *EOS Trans. Am. Geophys. Union*, **90**, 373–374.
- Kleinhans, M.G.** (2010) Sorting out river channel patterns. *Prog. Phys. Geogr.*, **34**(3), 287–326.
- Kostianoi, A. and Kosarev, A.** (2005) *The Caspian Sea Environment*. Springer-Verlag, Berlin, Heidelberg, New York, 271 pp.
- Kulp, M., Fitzgerald, D. and Penland, S.** (2005) Sand-rich lithosomes of the Holocene Mississippi River delta plain, in *River Deltas-Concepts, Models, and Examples. Spec. Publ. SEPM Soc. Sed. Geol.*, **83**, 279–293.
- Kumari, V.R. and Rao, I.M.** (2009) Estuarine characteristics of lower Krishna river. *Indian J. Mar. Sci.*, **38**(2), 215–223.
- Lazarus, E.D. and Constantine, J.A.** (2013) Generic theory for channel sinuosity. *Proc. Natl. Acad. Sci. USA*, **110**(21), 8447–8452.
- Leopold, L.B. and Langbein, W.B.** (1966) River meanders. *Sci. Am.*, **71**, 769–793.
- Leopold, L.B. and Wolman, M.G.** (1960) River meanders. *Geol. Soc. Am. Bull.*, **71**(6), 769–793.
- Lesser, G., Roelvink, J., Van Kester, J. and Stelling, G.** (2004) Development and validation of a three-dimensional morphological model. *Coastal Eng.*, **51**, 883–915.
- Li, G., Wei, H., Han, Y. and Chen, Y.** (1998) Sedimentation in the Yellow River delta, Part I: flow and suspended sediment structure in the upper distributary and the estuary. *Mar. Geol.*, **149**(1), 93–111.
- Li, Y., Jin, Z., Gao, B., Shi, L. and Li, G.** (2016) Sedimentary characteristics and quantitative parameters of sand bodies in distributary channel: a case study of Ganjiang delta in Poyang Lake. *J. Earth Sci. Environ.*, **38**, 306–316.
- Fadlillah, L.N., Widyastuti, M., Geotongsong, T., Sunarto and Marfai, M.A.** (2019) Hydrological characteristics of estuary in wulan delta in demak regency, indonesia. *Water Resour.*, **46**(6), 832–843.
- Luchi, R., Zolezzi, G. and Tubino, M.** (2011) Bend theory of river meanders with spatial width variations. *J. Fluid Mech.*, **681**, 311.
- Marciano, R., Wang, Z.B., Hibma, A., De Vriend, H.J. and Defina, A.** (2005) Modeling of channel patterns in short tidal basins. *J. Geophys. Res.*, **110**, F01001. <https://doi.org/10.1029/2003JF000092>.
- Marfai, M.A., Tyas, D.W., Nugraha, I., Fitriatul'Ulya, A. and Riasasi, W.** (2016) The Morphodynamics of Wulan Delta and Its Impacts on the Coastal Community in Wedung Subdistrict, Demak Regency, Indonesia. *J. Environ. Prot.*, **7**(1), 60–71.

- Mariotti, G., Falcini, F., Geleynse, N., Guala, M., Sun, T. and Fagherazzi, S.** (2013) Sediment eddy diffusivity in meandering turbulent jets: implications for levee formation at river mouths. *J. Geophys. Res. Earth Surf.*, **118**(3), 1908–1920.
- Nanson, G.C.** (1980) Point bar and floodplain formation of the meandering Beatton River, northeastern British Columbia, Canada. *Sedimentology*, **27**(1), 3–29.
- Nanson, G.C. and Croke, J.** (1992) A genetic classification of floodplains. *Geomorphology*, **4**, 459–486.
- Nienhuis, J.H., Ashton, A.D., Edmonds, D.A., Hoitink, A. and Törnqv, T.E.** (2020) Global-scale human impact on delta morphology has led to net land area gain. *Nature*, **577**(7791), 514–518.
- Nittrouer, J.A., Best, J.L., Brantley, C., Cash, R.W., Czapiga, M., Kumar, P. and Parker, G.** (2012) Mitigating land loss in coastal Louisiana by controlled diversion of Mississippi River sand. *Nat. Geosci.*, **5**, 534–537.
- Olariu, C. and Bhattacharya, J.P.** (2006) Terminal distributary channels and delta front architecture of river-dominated delta systems. *J. Sed. Res.*, **76**, 212–233.
- Paola, C.** (2001) Modeling stream braiding over a range of scales. In: *Gravel-bed Rivers V: Christchurch* (Ed. Mosley, M.P.), pp. 11–46. Caxton Press, Christchurch.
- Paola, C., Twilley, R.R., Edmonds, D.A., Kim, W., Mohrig, D., Parker, G., Viparelli, E. and Voller, V.R.** (2011) Natural processes in delta restoration: application to the Mississippi Delta. *Annu. Rev. Mar. Sci.*, **3**, 67–91.
- Parker, G., Sawai, K. and Ikeda, S.** (1982) Bend theory of river meanders. Part 2. Nonlinear deformation of finite-amplitude bends. *J. Fluid Mech.*, **115**, 303–314.
- Peakall, J., Ashworth, P.J. and Best, J.L.** (2007) Meander-bend evolution, alluvial architecture, and the role of cohesion in sinuous river channels: a flume study. *J. Sed. Res.*, **77**(3), 197–212.
- Penland, S., Connor, P.F., Beall, A., Fearnley, S. and Williams, S.J.** (2005) Changes in Louisiana's shoreline: 1855–2002. *J. Coastal Res.*, **44**, 7–39.
- Postma, G.** (1990) An analysis of the variation in delta architecture. *Terra Nova*, **2**, 124–130.
- Poulos, S., Collins, M.B. and Ke, X.** (1993) Fluvial/wave interaction controls on delta formation for ephemeral rivers discharging into microtidal waters. *Geo-Mar. Lett.*, **13**, 24–31.
- Rao, P.S., Rao, G.K., Rao, N.V.N.D. and Swamy, A.S.R.** (1990) Sedimentation and sea-level variations in Nizampatnam Bay, East-Coast of India. *Indian J. Mar. Sci.*, **19**, 261–264.
- Rego, J.L., Meselhe, E., Stronach, J. and Habib, E.** (2010) Numerical modeling of the Mississippi–Atchafalaya Rivers' sediment transport and fate: considerations for diversion scenarios. *J. Coastal Res.*, **26**, 212–229.
- Rhoads, B.L. and Welford, M.R.** (1991) Initiation of river meandering. *Prog. Phys. Geogr.*, **15**(2), 127–156.
- van Rijn, L.C.** (1993) *Principles of Sediment Transport in Rivers, Estuaries, and Coastal Seas*. Aqua publications, Amsterdam, 615 pp.
- Rowland, J.C., Dietrich, W.E., Day, G. and Parker, G.** (2009) Formation and maintenance of single-thread tie channels entering floodplain lakes: observations from three diverse river systems. *J. Geophys. Res.*, **114**, F02013.
- Rowland, J.C., Dietrich, W.E. and Stacey, M.T.** (2010) Morphodynamics of subaqueous levee formation: insights into river mouth morphologies arising from experiments. *J. Geophys. Res. Earth Surf.*, **115**, F04007.
- Rust, B.R.** (1978) Depositional models for braided alluvium. *Fluvial Sedimentol.*, **5**, 605–625.
- Schuurman, F., Marra, W.A. and Kleinhans, M.G.** (2013) Physics-based modeling of large braided sand-bed rivers: bar pattern formation, dynamics, and sensitivity. *J. Geophys. Res. Earth Surf.*, **118**, 2509–2527.
- Schuurman, F., Shimizu, Y., Iwasaki, T. and Kleinhans, M.G.** (2016) Dynamic meandering in response to upstream perturbations and floodplain formation. *Geomorphology*, **253**, 94–109.
- Seminara, G. and Tubino, M.** (1989) Alternate bars and meandering: free, forced and mixed interactions. *River Meandering*, **12**, 267–320.
- Shankman, D., Keim, B.D. and Song, J.** (2006) Flood frequency in China's Poyang Lake region: trends and teleconnections. *Int. J. Climatol.*, **26**, 1255–1266.
- Smith, D.G., Hubbard, S.M., Lavigne, J.R., Leckie, D.A. and Fustic, M.** (2011) Stratigraphy of counter-point bar and eddy-accretion deposits in low energy meander belts of the Peace-Athabasca delta, northeast Alberta, Canada. In: *River to Rock* (Ed. North, C.), *SEPM Special Publication*, **97**, 143–152.
- Smith, N.** (1974) Sedimentology and bar formation in the Upper Kicking Horse River, a braided outwash stream. *J. Geol.*, **82**, 205–223.
- Socolofsky, S.A. and Jirka, G.H.** (2004) Large-scale flow structures and stability in shallow flows. *J. Environ. Eng. Sci.*, **3**(5), 451–462.
- Solari, L., Seminara, G., Lanzoni, S., Marani, M. and Rinaldo, A.** (2002) Sand bars in tidal channels Part 2. Tidal meanders. *J. Fluid Mech.*, **451**, 203.
- Stoesser, T., Ruether, N. and Olsen, N.R.B.** (2010) Calculation of primary and secondary flow and boundary shear stresses in a meandering channel. *Adv. Water Resour.*, **33**(2), 158–170.
- Strick, R.J., Ashworth, P.J., Awcock, G. and Lewin, J.** (2018) Morphology and spacing of river meander scrolls. *Geomorphology*, **310**, 57–68.
- Sylvester, Z., Durkin, P. and Covault, J.A.** (2019) High curvatures drive river meandering. *Geology*, **47**(3), 263–266.
- Syvitski, J.P.M., Kettner, A.J., Overeem, I., Hutton, E.W.H., Hannon, M.T., Brakenridge, G.R., John, D., Charles, V., Yoshiki, S., Liviu, G. and Robert, J.N.** (2009) Sinking deltas due to human activities. *Nat. Geosci.*, **2**, 681–686.
- Syvitski, J.P.M. and Saito, Y.** (2007) Morphodynamics of deltas under the influence of humans. *Global Planet. Change*, **57**, 261–282.
- Tal, M. and Paola, C.** (2007) Dynamic single-thread channels maintained by the interaction of flow and vegetation. *Geology*, **35**, 347–350.
- Tan, Q.** (1982) The historical process of the evolution of Poyang Lake. *J. Fudan Univ. Soc. Sci.*, **2**, 42–51.
- Tejedor, A., Longjas, A., Caldwell, R., Edmonds, D.A., Zaliapin, I. and Foufoula-Georgiou, E.** (2016) Quantifying the signature of sediment composition on the topologic and dynamic complexity of river delta channel networks and inferences toward delta classification. *Geophys. Res. Lett.*, **43**, 3280–3287.
- Thomas, R.L., Christensen, M.D., Szalinska, E. and Scarlat, M.** (2006) Formation of the St. Clair River Delta in the Laurentian Great Lakes System. *J. Great Lakes Res.*, **32**(4), 738–748.
- Timoney, K. and Lee, P.** (2016) Changes in the areal extents of the Athabasca River, Birch River, and Cree Creek

- Deltas, 1950–2014, Peace-Athabasca Delta, Canada. *Geomorphology*, **258**, 95–107.
- Törnqvist, T.E., Wallace, D.J., Storms, J.E.A., Wallinga, J., van Dam, R.L., Blaauw, M., Derksen, M.S., Klerks, C.J.W., Meijneken, C. and Snijders, E.M.A.** (2008) Mississippi Delta subsidence primarily caused by compaction of Holocene strata. *Nat. Geosci.*, **1**, 173–176.
- Usman, M.** (2016) On consistency and limitation of independent t-test Kolmogorov Smirnov Test and Mann Whitney U test. *IOSR-JM*, **12**(4), 22–27.
- Van der Wegen, M. and Roelvink, J.A.** (2012) Reproduction of estuarine bathymetry by means of a process-based model: Western Scheldt case study, the Netherlands. *Geomorphology*, **179**, 152–167.
- Wang, Y., Storms, J.E.A., Martinius, A.W., Karsenberg, D. and Abels, H.A.** (2020) Evaluating alluvial stratigraphic response to cyclic and non-cyclic upstream forcing through process-based alluvial architecture modelling. *Basin Res.*, **33**(1), 48–65.
- Willis, B. and Sun, T.** (2019) Relating depositional processes of river-dominated deltas to reservoir behavior using computational stratigraphy. *J. Sed. Res.*, **89**(12), 1250–1276.
- Woodbridge, K.P.** (2013) *The influence of Earth surface movements and human activities on the River Karun in lowland south-west Iran*. PhD thesis, University of Hull, Hull, 324 pp.
- Wright, L.D.** (1977) Sediment transport and deposition at river mouths: a synthesis. *Geol. Soc. Am. Bull.*, **88**, 857–868.
- Wu, S., Xu, Z. and Liu, Z.** (2019) Depositional architecture of fluvial-dominated shoal water delta. *J. Palaeogeogr.*, **21** (02), 202–215.
- Xu, D., Xiong, M. and Zhang, J.** (2001) Analysis on hydrologic characteristics of Poyang Lake. *Yang. Riv.*, **32**, 21–27.
- Xu, Z.H., Wu, S.H., Liu, Z., Zhao, J.S., Wu, J.C., Geng, L.H., Zhang, T.Y. and Liu, Z.W.** (2019) Reservoir architecture of the finger bar within shoal water delta front: insights from the Lower Member of Minghuazhen Formation, Neogene, Bohai BZ25 Oilfield, Bohai Bay Basin, East China. *Pet. Explor. Dev.*, **46**, 1–12.
- Yin, Z. and Zhang, J.** (1987) The hydrological features of Poyang Lake. *Oceanol. Limnol. Sinica*, **18**, 22–27.
- Zhang, J., Wang, M., Wang, Y., Jiang, Y., Lei, Y., Zhang, L. and Wang, J.** (2017) Identification and sedimentary evolution of the shallow water delta of bird-foot in Bozhong 28–2S Oilfield Group of Bohai Bay Basin. *Period. Ocean Univ. China*, **47**(9), 77–85.
- Zhang, Y., Bao, Z., Dou, L., Jiang, L., Wei, M. and Zhang, L.** (2020) Hydrodynamics and deposition in lacustrine shallow-water delta front: a combination of numerical simulations and modern sedimentation measurements. *Interpretation*, **8**(3), 1–14.

Manuscript received 3 November 2020; revision accepted 22 July 2021